JOURNAL OF COMPUTATIONAL PHYSICS 108, 272–295 (1993)

The Stability of Numerical Boundary Treatments for Compact High-Order Finite-Difference Schemes

MARK H. CARPENTER

Theoretical Flow Physics Branch, Fluid Mechanics Division, NASA Langley Research Center, Hampton, Virginia 23681

DAVID GOTTLIEB

Division of Applied Mathematics, Brown University, Providence, Rhode Island 02912

AND

SAUL ABARBANEL

Department of Mathematical Sciences, Division of Applied Mathematics, Tel-Aviv University, Tel-Aviv, Israel

Received October 17, 1991; revised January 29, 1993

The stability characteristics of various compact fourth- and sixth-order spatial operators are assessed with the theory of Gustafsson, Kreiss, and Sundström (G–K–S) for the semidiscrete initial boundary value problem. These results are generalized to the fully discrete case with a recently developed theory of Kreiss and Wu. In all cases, favorable comparisons are obtained between G–K–S theory, eigenvalue determination, and numerical simulation. The conventional definition of stability then is sharpened to include only those spatial discretizations that are asymptotically stable (bounded, left half-plane eigenvalues). Many of the higher order schemes that are G–K–S stable are not asymptotically stable. A series of compact fourth- and sixth-order schemes that are both asymptotically and G–K–S stable for the scalar case are then developed.

INTRODUCTION

Recently, higher order numerical methods have seen increasing use in the direct numerical simulation (DNS) of the Navier–Stokes equations. Although these methods do not have the spatial resolution of spectral methods, they offer significant increases in accuracy over conventional, second-order methods. These methods are generally more robust and less costly than spectral methods. The issue of the relative cost of various higher order schemes (accuracy weighted against physical and numerical cost) is a complex issue that is ultimately dependent on what features of the solution are sought and how accurately they must be resolved. In any event, further development of the underlying stability theory of these schemes is important.

The state of higher order temporal discretizations is well developed and relies greatly on the existing ordinary differential equation (ODE) literature. Higher order spatial discretizations are also well documented in the literature. For example, entire classes of centered explicit spatial schemes are described in the text of Kopal [1]. In practice, compact schemes (methods in which both the solution and its derivatives are treated as unknowns and are solved for simultaneously) are more accurate than optimal explicit schemes (Nth-order schemes that involve $N+1$ grid points) and have recently gained much attention for use in DNS. The fundamental ideas of compact schemes, as well as derivation techniques, can be found in the work of Vichnevetsky [2] and will not be pursued in this work. The primary difficulty in using higher order schemes is identification of stable boundary schemes that preserve their formal accuracy. For a hyperbolic system to preserve formal spatial accuracy, an Nth-order inner scheme must be closed with at least an $(N-1)$th-order boundary scheme [3]. To date, many higher order inner schemes are used with lower order boundary schemes because no stable, higher order formulations are known. The formal accuracy of these formulations is thus reduced to one order more than the boundary condition (BC) accuracy, so that the additional

0021-9991/93 $5.00

work incurred with the higher order inner scheme is difficult to justify.

Determination of the numerical stability of a fully discrete approximation for a linear hyperbolic partial-differential equation is a difficult task. For the Cauchy problem on an infinite domain $(-\infty, \infty)$, standard techniques based on Fourier methods generally provide the necessary conditions for stability of the numerical scheme. For the initial boundary value problem (IBVP) on the semiinfinite domain $[0, \infty)$, or the finite domain $[-1, 1]$, Fourier techniques are not straightforward to apply and do not provide sufficient conditions for numerical stability. To address these issues, Osher [4], Kreiss [5], and later Gustafsson *et al.* [6] developed stability analysis techniques based on normal modal analysis. Their work (generally referred to as G–K–S stability theory) established conditions that the inner and boundary schemes must satisfy to ensure stability. The G–K–S theory states that hyperbolic systems are assumed stability if no eigenvalues or generalized eigenvalues exist for the IBVP. Trefethen [7] further clarified the physical meaning of the G–K–S condition by noting that the concept of stability at a boundary could be related to the group velocity of the boundary scheme (specifically, whether energy is carried into or out of the numerical domain).

One of the weak points of fully discrete G–K–S theory has been the complexity in its application to higher order numerical schemes. If the spatial or temporal accuracy is raised, then the complexity of the polynomials that govern the stability of the numerical approximation is generally increased (the order increases, which gives rise to more roots). In multistage time discretization schemes (e.g., Runge-Kutta (R–K) schemes with three or more stages), where boundary conditions must be applied at intermediate levels, the stability polynomials that must be tested at each boundary are nearly insurmountable with analytic techniques. The analysis can be simplified by addressing the semidiscrete problem as a method-of-lines IBVP rather than the fully discrete problem. The underlying G–K–S theory for the semidiscrete problem was initially developed by Strikwerda [8]. He showed that by discretizing space and leaving time continuous, the necessary and sufficient conditions for method-of-lines IBVP stability are analogous to those that govern the stability of the fully discrete case.

The precise connection between the semidiscrete stability bounds and those obtained in the fully discrete analysis is not always straightforward. Recently, however, Kreiss *et al.* [10] have shown that under very weak conditions, stability of the semidiscrete approximation infers stability in the fully discrete approximation if specific R–K time-marching schemes are used. Therefore, the semidiscrete G–K–S theory can be relied on to assess the stability with R–K integration of various higher order spatial discretization operators, which simplifies the calculations considerably.

There are other methods for establishing boundary stability for the IBVP, most notably the work of Goldberg and Tadmor (e.g., [9]). They have addressed the complexity of G–K–S analysis by devising more versatile and convenient stability criteria for wide classes of finite-difference approximations. Unfortunately, the discretizations we are considering fall outside of the validity of their work since we are not using translatory boundary conditions for the spatial operator.

The emphasis of this work is to apply semidiscrete G–K–S theory to several higher order spatial operators for the IBVP. Because compact methods naturally lend themselves to fewer implementational difficulties at the boundaries, these methods will be the primary focus. Stable boundary formulations that preserve the formal accuracy of the inner scheme will be presented for spatial derivative operators of up to sixth order.

MODEL EQUATION FOR IBVP

The Euler equations of fluid dynamics in one spatial dimension can be written as a system of hyperbolic equations with the form

$$\frac{\partial U}{\partial t} = A\frac{\partial U}{\partial x} + F, \qquad x \geqslant 0, \qquad t \geqslant 0, \tag{1}$$

where A is a matrix with real eigenvalues, F is a source term, and boundary and initial data are supplied in the form

$$U^{\mathrm{I}}(0, t) + TU^{\mathrm{II}}(0, t) = g(t), \qquad U(x, 0) = f(x), \tag{2}$$

where T is a matrix that describes the boundary conditions. The problem is well posed if the solution $U(x, t)$ depends smoothly on the initial and boundary data. The focus in this work will be on the scalar form of Eqs. (1) and (2), where the matrix A is a negative real constant a and the source term is $F = 0$. This simplification can be justified because stability of a numerical scheme on the scalar equation implies stability of the system if boundary conditions are imposed in a characteristic form (e.g., Gottlieb *et al.* [11]).

SEMIDISCRETIZATION

In this work, the numerical discretization of Eq. (1) will be accomplished in two separate steps. The spatial derivatives first will be approximated with appropriate formulas, which leaves what is generally referred to as a semidiscretization. The numerical solution will then be advanced

in time in a method-of-lines approach with a stable temporal scheme. The continuous domain $[0, 1]$ is divided into N uniform intervals of width Δx, where $N\Delta x = 1$. The continuous derivative U_x is then replaced with a finite-difference representation that involves the functional values U_j at the discrete points. A system of ODEs results in the form

$$\frac{dV}{dt} = M^+ V, \tag{3}$$

where

$$M^+ V_j = \sum_{k=-L_j}^{R_j} am_j^k V_{j+k}, \qquad j = 0, ..., N \tag{4}$$

and L and R are the width of the stencil that extends to the left and right of grid point j, respectively. Note that m_j^k, L_j, and R_j are functions of j. Consider the case where the same spatial stencil is used at every interior grid point in the domain such that $L_j = L$ and $R_j = R$. This scheme can only be used for $L < j < N - R$ since for other values of j, the stencil protrudes through the boundary. Thus, exactly $L + R$ additional formulas have to be defined near the boundaries. Because only one physical boundary condition exists, $L + R - 1$ of the schemes are strictly numerically motivated. These schemes are generally referred to as numerical boundary schemes (NBS).

The physical boundary condition $g(t)$ is imposed at the grid point $j = 0$, and Eq. (3) can be rewritten as

$$\frac{dV}{dt} = MV + Bg(t), \tag{5}$$

where M is an $N \times N$ matrix and B is a vector of dimension N, which describes the dependence of the jth scheme on the boundary data. The matrix M usually is diagonal of order $L + R + 1$ for most explicit methods, but can in general be full. For stability analysis, $g(t)$ can be set to zero with little loss of generality. The exact solution of the semidiscretization described by Eq. (5) for homogeneous boundary data becomes

$$V(t) = f(x)\, e^{Mt}. \tag{6}$$

The stability of the numerical scheme depends on the properties of M, which includes information from the interior and boundary discretizations.

These points about boundary closures can be clarified with examples of explicit and implicit spatial schemes. Concentration will be on schemes that have at least fourth-order spatial accuracy because most of the difficulties associated with high-order stencils are not observed with second-order schemes. The first is an explicit five-point scheme reported by Gary [12] and later shown by Strikwerda [8] to be G–K–S stable. The scheme is uniformly fourth order in space. The spatial discretization is accomplished with the stencils

$$\frac{\partial V_0}{\partial x} = \frac{1}{12\,\Delta x}(-25V_0 + 48V_1 - 36V_2 + 16V_3 - 3V_4)$$

$$\frac{\partial V_1}{\partial x} = \frac{1}{12\,\Delta x}(-3V_0 - 10V_1 + 18V_2 - 6V_3 + V_4)$$

$$\frac{\partial V_j}{\partial x} = \frac{1}{12\,\Delta x}(V_{j-2} - 8V_{j-1} + 8V_{j+1} - V_{j+2})$$

$$(j = 2, ..., N-2)$$

$$\frac{\partial V_{N-1}}{\partial x} = \frac{1}{12\,\Delta x}(-V_{N-4} + 6V_{N-3} - 18V_{N-2} + 10V_{N-1} + 3V_N)$$

$$\frac{\partial V_N}{\partial x} = \frac{1}{12\,\Delta x}(3V_{N-4} - 16V_{N-3} + 36V_{N-2} - 48V_{N-1} + 25V_N). \tag{7}$$

The terms in Eq. (3) take the form

$$V^+ = \begin{bmatrix} V_0 \\ V_1 \\ V_2 \\ V_3 \\ \vdots \\ V_{N-2} \\ V_{N-1} \\ V_N \end{bmatrix},$$

$$\hat{M}^+ = \begin{bmatrix} -25 & 48 & -36 & 16 & -3 & & & & & \\ -3 & -10 & 18 & -6 & 1 & & & & & \\ 1 & -8 & 0 & 8 & -1 & & & & 0 & \\ & 1 & -8 & 0 & 8 & -1 & & & & \\ & & \cdot & \cdot & \cdot & \cdot & \cdot & \cdot & & \\ & & & & & & & & & \\ & & & & & 1 & -8 & 0 & 8 & -1 \\ & & 0 & & & -1 & 6 & -18 & 10 & 3 \\ & & & & & 3 & -16 & 36 & -48 & 25 \end{bmatrix}, \tag{8}$$

where $M^+ = (a/12\,\Delta x)\,\hat{M}^+$. Four NBSs are required to close the numerical scheme, only one of which will be overwritten by a physical boundary condition. The boundary

condition is accounted for at the grid point $j=0$ in Eq. (8), which results in expressions for Eq. (5) of the form

$$V=\begin{bmatrix} V_1 \\ V_2 \\ V_3 \\ \vdots \\ V_{N-2} \\ V_{N-1} \\ V_N \end{bmatrix},$$

$$\hat{M}=\begin{bmatrix} -10 & 18 & -6 & 1 & & & & & \\ -8 & 0 & 8 & -1 & & & & 0 & \\ 1 & -8 & 0 & 8 & -1 & & & & \\ & \ddots & \ddots & \ddots & \ddots & \ddots & \ddots & & \\ & & & & 1 & -8 & 0 & 8 & -1 \\ & 0 & & & -1 & 6 & -18 & 10 & 3 \\ & & & & 3 & -16 & 36 & -48 & 25 \end{bmatrix},$$

$$\hat{B}=\begin{bmatrix} -3 \\ 1 \\ 0 \\ \vdots \\ 0 \\ 0 \\ 0 \end{bmatrix}, \tag{9}$$

where $M=(a/12\,\Delta x)\,\hat{M}$ and $B=(a/12\,\Delta x)\,\hat{B}$. The matrix M is the $N\times N$ submatrix of the matrix M^+, which corresponds to $1\leqslant i, j\leqslant N$.

The implicit fourth-order example is a compact discretization in which the numerical approximation to $\partial U_j/\partial x$ is made in the form

$$\begin{aligned} &\frac{\partial V_0}{\partial x}+3\frac{\partial V_1}{\partial x} \\ &\quad=\frac{1}{6\,\Delta x}(-17V_0+9V_1+9V_2-V_3) \\ &\frac{\partial V_{j-1}}{\partial x}+4\frac{\partial V_j}{\partial x}+\frac{\partial V_{j+1}}{\partial x} \\ &\quad=\frac{1}{\Delta x}(-3V_{j-1}+3V_{j+1}) \\ &3\frac{\partial V_{N-1}}{\partial x}+\frac{\partial V_N}{\partial x} \\ &\quad=\frac{1}{6\,\Delta x}(V_{N-3}-9V_{N-2}-9V_{N-1}+17V_N). \end{aligned} \tag{10}$$

In matrix notation, Eq. (10) is often expressed in the form $M_1^+(dV/dx)=M_2^+V$, where $M^+=(M_1^+)^{-1}M_2^+$, and

$$V^+=\begin{bmatrix} V_0 \\ V_1 \\ \vdots \\ V_{N-1} \\ V_N \end{bmatrix},$$

$$M_1^+=\begin{bmatrix} 6 & 18 & & & & & \\ 1 & 4 & 1 & & & 0 & \\ & \ddots & \ddots & \ddots & & & \\ & & & \ddots & \ddots & \ddots & \\ & 0 & & & 1 & 4 & 1 \\ & & & & & 18 & 6 \end{bmatrix},$$

$$\hat{M}_2^+=\begin{bmatrix} -17 & 9 & 9 & -1 & & & \\ -3 & 0 & 3 & & & 0 & \\ & \ddots & \ddots & \ddots & & & \\ & & & \ddots & \ddots & \ddots & \\ & 0 & & & -3 & 0 & 3 \\ & & & & 1 & -9 & -9 & 17 \end{bmatrix}, \tag{11}$$

where $M_2^+=(a/\Delta x)\,\hat{M}_2$. The boundary information is imposed at grid joint $j=0$ to reduce the matrix by one order and to yield matrix equations for the reduced vector V of the form

$$M_1=\begin{bmatrix} 6 & 6 & & & & & \\ 1 & 4 & 1 & & & 0 & \\ & \ddots & \ddots & \ddots & & & \\ & & & \ddots & \ddots & \ddots & \\ & 0 & & & 1 & 4 & 1 \\ & & & & & 18 & 6 \end{bmatrix},$$

$$\hat{M}_2=\begin{bmatrix} -1 & 9 & 9 & & & & \\ -3 & 0 & 3 & & & 0 & \\ & \ddots & \ddots & \ddots & & & \\ & & & \ddots & \ddots & \ddots & \\ & 0 & & & -3 & 0 & 3 \\ & & & & 1 & -9 & -9 & 17 \end{bmatrix}, \tag{12}$$

$$\hat{B}_2=\begin{bmatrix} -1 \\ 0 \\ \vdots \\ 0 \\ 0 \end{bmatrix},$$

where $B_2=(a/\Delta x)\,\hat{B}_2$. Because a matrix multiplication was used to determine the spatial operator for grid points $1\leqslant j\leqslant N$, matrix M is not a simple submatrix of matrix M^+ as it was with the explicit scheme. The spatial operator described by Eq. (12) is compact because both M_1 and M_2 involve only three grid points (except near the boundary in

M_2). Because of this compactness, $L = R = 1$ and only two NBSs must be defined (one of which includes, but is not replaced by, the physical boundary condition). This algorithm expressed in the form of Eq. (5) yields

$$M = M_1^{-1} M_2, \qquad B = M_1^{-1} B_2. \tag{13}$$

Although the algorithm is implementationally compact, the resulting M is a full $N \times N$ matrix.

The structure of the two spatial discretizations described thus far and all of the discretizations analyzed in this work have the property of "asymmetry." Specifically, a central difference scheme is used in the interior of the domain, and identical NBSs are used at both ends of the spatial operator. (This is the property which yields the work of Goldberg and Tadmor inapplicable.) With this property the matrix M defined by Eq. (5) is identical (to within a sign) regardless of which end of the domain the physical boundary condition is applied. Therefore, stability is guaranteed for both positive and negative wave speeds. This is important from a practical point of view because the signs of the eigenvalues of the matrix A in Eq. (1) are not known a priori for a hyperbolic system. Typically, the numerical solution is advanced in time for the entire domain $j = 0, N$, followed by a characteristic decomposition. The boundary conditions are imposed at either $j = 0$ or $j = N$, depending on the signs of the eigenvalues so that the resulting system is well posed.

For future reference, a convenient nomenclature is defined to describe these matrices. Let matrix M^+ be described as $(NBS_1, ..., NBS_L - CD - NBS_R, ..., NBS_N)$, where CD is the order of the central-difference operator used in the interior and NBS_j is the order of the NBS used at each of the points next to the boundary. For example, the explicit, uniformly fourth-order scheme represented by matrix equation (8) is denoted by the nomenclature (4, 4–4–4, 4), where the –4– denotes the inner scheme that is approximated with a fourth-order stencil and the symmetric 4, 4 denotes fourth-order stencils at $j = 0, 1,$ and $j = N - 1, N$. The three-point compact scheme described by Eq. (11) is denoted (4–4–4). Again, the –4– refers to the inner-scheme accuracy, and the symmetric 4's indicate closure on the boundaries of fourth-order accuracy. No ambiguity exists in the nomenclature between the compact and explicit schemes since only the compact scheme can retain fourth-order inner accuracy with one NBS at each boundary.

STABILITY OF THE IBVP

The eigenvalues of matrix M from Eq. (5) which result from higher order finite-difference approximations of U_x align along the imaginary axis in complex conjugate pairs. To time advance Eq. (5) efficiently, the time discretization algorithm should include a large portion of the imaginary axis in its stability domain. Conventional R–K time-advancement algorithms of third or fourth order are well suited for semidiscretizations of hyperbolic equations and are the only method considered in this study. In particular, the standard fourth-order method of Kutta (e.g., Gear [13]) will be used in this study because of the fourth-order nonlinear accuracy, the large stability envelope, and the low storage requirements.

Our objective is to analytically determine the stability of various higher order spatial discretizations advanced with the fourth-order R–K time scheme. Conventional G–K–S theory for the fully discrete IBVP with a second-order space discretization involves solving polynomials of eighth order in κ at the boundaries. Closed-form solutions are difficult to obtain under these circumstances and are more complicated with increasing spatial accuracy. The analysis can be greatly simplified by relying on three fundamental theorems of stability analysis that are valid for the conditions in this study. Each will be discussed briefly, but for further clarification, the original works should be consulted. The essential elements of the theorems that form the basis of this work follow.

THEOREM 1. *G–K–S theory (fully discrete [6] or semidiscrete [8]) asserts that to show stability for the finite-domain problem, the inner scheme must be Cauchy stable on* $(-\infty, \infty)$, *and that each of the two quarter-plane problems must be stable with the use of normal modal analysis. Thus, the stability of the finite-domain problem is broken into the summation of three simpler problems.*

THEOREM 2. *For each quarter-plane problem that arises in Theorem* 1, *a necessary and sufficient condition for stability of the IBVP is that no eigensolution exists. This theorem is true for either the fully discrete case* [6] *or the semidiscrete case* [8].

The algebraic complexity involved in showing stability of the IBVP is dramatically reduced in the semidiscrete case because time remains continuous. Ultimately, numerical stability is a fully discrete concept, and a connection between the semidiscrete and fully discrete stabilities must be used. The third theorem provides this connection.

THEOREM 3. *Under mild restrictions* [10], *if a semidiscrete approximation is stable in a generalized sense and an R–K method that is locally stable is used to time march the semidiscretization, then the resulting totally discrete approximation is stable in the same sense as long as the stability region of the R–K method encompasses the norm of the semidiscretization.*

The stability definitions [10] used in the first two theorems (G–K–S stability) are different than that used in the third (generalized stability). The first two theorems rely

on G–K–S stability (sometimes referred to as the Kreiss condition) in the semi discrete and fully discrete cases. At least two different definitions of G–K–S stability are encountered in the works concerning G–K–S analysis. The subtle differences between these definitions of stability will not affect the conclusions in this work, and the terms G–K–S stability and Lax stability will be used interchangeably. We now describe in some detail the implications of the three theorems.

Because Fourier methods are not well suited for the finite domain, stability analysis can be carried out by energy methods, matrix methods, or by normal modal analysis. Energy and matrix methods are, in general, difficult to perform on high-order schemes. The modal relationships are simple to define, but analytic solutions are often intractable. Theorem 1 describes how G–K–S analysis can be used to augment finite domain model analysis. The original finite-domain modal analysis is broken into the analysis of three equivalent, yet simpler, modal problems. With the assumption that a Cauchy-stable scheme is used for the interior grid points, the inner scheme is tested for stability at each boundary in a semi-infinite spatial domain. In so doing, the stability of each boundary is independent of the influence from the other boundary. Stability of the two boundary problems implies stability of the finite-domain numerical method. In addition, Theorem 1 provides a perturbation test for generalized eigensolutions. The test establishes the stability of certain borderline cases in normal modal analysis.

To fully appreciate the power of G–K–S analysis, a normal modal analysis of the fourth-order compact scheme (4–4–4) described by Eq. (12) is presented for the coupled finite-domain problem. We proceed with the assumption that the semidiscrete problem defined in Eq. (5) has a solution of the form

$$V_j(t) = e^{St}\phi_j, \tag{14}$$

where S are the eigenvalues of the matrix $M_1^{+-1}M_2^+$. Substitution into Eq. (5) yields the generalized eigenvalue problem

$$M_1^+ S V_j = M_2^+ V_j \tag{15}$$

for which we have assumed $g(t) = 0$. The resolvent equation provided by the inner scheme is

$$(\phi_{j-1} + 4\phi_j + \phi_{j+1})\,\hat{S} = 3(-\phi_{j-1} + \phi_{j+1}),$$
$$j = 2, \ldots, N-1, \tag{16}$$

where $S = (a/\Delta x)\,\hat{S}$. Assuming $\phi_j = \phi_o \kappa^j$ yields the following equation for the eigenvalues:

$$\left(\frac{1}{\kappa} + 4 + \kappa\right)\hat{S} = 3\left(\frac{-1}{\kappa} + \kappa\right). \tag{17}$$

This is a quadratic expression in κ, which will in general have two solutions which satisfy Eq. (17). Therefore, the eigenvectors are of the form $\phi_j = C_1\kappa_1^j + C_2\kappa_2^j$. Simple manipulations show that the two roots are related by

$$\kappa_1 = \kappa, \qquad \kappa_2 = \frac{-2-\kappa}{2\kappa+1} \tag{18}$$

and

$$\phi_j = C_1\kappa^j + C_2\left(\frac{-2-\kappa}{2\kappa+1}\right)^j. \tag{19}$$

We note that if $\kappa = a + ib$, then

$$|\kappa_1| = a^2 + b^2, \qquad |\kappa_2| = \frac{b^2 + (a+2)^2}{(2b)^2 + (2a+2)^2} \tag{20}$$

and $|\kappa_1| \geqslant 1$ implies $|\kappa_2| \leqslant 1$. Thus, each κ is dominant near one of the boundaries, and its influence decays monotonically as the distance from that boundary increases. The forms of C_1 and C_2 must be determined from the boundary conditions at $j = 1$ and $j = N$. The conditions at the two boundaries can be represented as

$$\begin{aligned} C_1[\hat{S} - F_1(\kappa_1)] + C_2[\hat{S} - F_1(\kappa_2)] &= 0 \\ C_1[\hat{S} - F_N(\kappa_1)] + C_2[\hat{S} - F_N(\kappa_2)] &= 0, \end{aligned} \tag{21}$$

where F_1 and F_N are the functional relations that result from substituting $V_j(t) = e^{St}\psi_j$ with $\psi_j = C_1\kappa_1^j + C_2\kappa_2^j$ into the expressions at grid points $j = 1$ and $j = N$, respectively. Note that $\hat{S} = \hat{S}(\kappa)$ and every term is a function of κ. No general solution to this problem exists with the exception of the trivial one. Nonzero solutions exist for the condition in which the determinant is equal to zero. The determinant condition gives an expression for κ. The roots of this expression, with Eqs. (17) and (19), give the eigenvalues and eigenvectors of the system.

No closed-form expressions are known for the roots of the determinant polynomial in this case or for any other reasonable boundary closures. To find the numerical solution of the determinant polynomial, the roots of an Nth-order polynomial in κ must be found, and numerical techniques must be used. (Note that this is equivalent to casting the original matrix operator as an eigenvalue problem.) The power of G–K–S theory results from breaking

the normal modal problem into three separate problems. The roots to the κ polynomials do not depend on the boundary-to-boundary coupling that is inherent in Eqs. (20) and (21).

Theorem 2 describes what constitutes stability for the two IBVPs in Theorem 1 for the fully discrete or the semidiscrete case and states that Eq. (1) must satisfy the condition that no eigenvalues or generalized eigenvalues exist. Both Theorems 1 and 2 rely on a definition of an eigensolution for their quarter-plane analysis. Here, an eigensolution is presented for the semidiscrete case. Similar definitions exist for the fully discrete case.

DEFINITION 1. An eigensolution for the IBVP defined by Eq. (5) is the nontrivial function $V(x, s)$, which satisfies [8]:

I. $SV = MV \ (x \geqslant 0)$

II. $V^{\mathrm{I}}(0, S) - TV^{\mathrm{II}}(0, S) = 0$

III. $\mathscr{R}(S) \geqslant 0$

IV. For $\mathscr{R}(S) > 0$, $V(x, S)$ is bounded as $x \to \infty$

V. For $\mathscr{R}(S) = 0$ and $|\kappa| = 1$, a perturbation inside the unit circle of κ ($|\kappa| = 1 - \varepsilon$, $\varepsilon > 0$) produces an eigenvalue $\mathscr{R}(S) > \delta$, $\delta > 0$.

Because $\psi = \psi_o \kappa^j$, condition IV implies $|\kappa| < 1$.

An eigensolution satisfying condition IV or V is referred to as a G–K–S eigenvalue or a generalized G–K–S eigenvalue, respectively. With these conditions, the test for numerical stability has been simplified from the coupled normal modal analysis to tests that involve $\mathscr{R}(S) > 0$ for $|\kappa| < 1$ at each boundary and the exceptional case when $\mathscr{R}(S) = 0$ and $|\kappa| = 1$.

Theorem 3 relates the stability of the semidiscretization to that of the fully discrete numerical method and relies on temporal advancement schemes that are locally stable. For a locally stable numerical method, the stability envelope $|z| \leqslant 1$ (z is the amplification factor) in the complex plane encompasses within the left half-plane (LH-P) an open semicircle of radius R_1 centered at the origin and symmetric about the real axis. The standard fourth-order R–K method satisfies this condition. A discretization of time with the fourth-order R–K method in Eq. (5) produces a fully discrete method defined by

$$\hat{V}(t + k) = L(kM)\, \hat{V}(t) + L(k)\, Bg(t), \tag{22}$$

where the time step $\Delta t = k$ and where $L(kM)$ is the polynomial in kM and describes the time discretization. Under very mild restrictions (see Kreiss [10]) on the eigenvalue structure of the matrix $L(kM)$ and if the semidiscrete approximation is stable in a generalized sense, then the totally discrete approximation is stable in the same sense for $\|kM\| < R_1$.

We have outlined a systematic approach to address the finite-domain stability problem for the fully discrete numerical approximation to Eq. (1). The remainder of this work will describe the application of these techniques to several higher order finite-difference schemes.

FOURTH-ORDER BOUNDARY CONDITIONS

Before the stability analysis of various higher order boundary conditions is presented, an example illustrates the necessity of $(N-1)$th-order boundary closure for an Nth-order inner scheme. The example also provides a numerical test to verify that G–K–S theory accurately predicts the stability behavior of the various numerical schemes. Consider the method-of-lines approximation to the scalar wave equation

$$\frac{\partial U}{\partial t} + \frac{\partial U}{\partial x} = 0, \qquad -1 \leqslant x \leqslant 1, \qquad t \geqslant 0 \tag{23}$$

$$\begin{aligned} U(t, -1) &= \sin 2\pi(-1 - t), \\ U(0, x) &= \sin 2\pi x, \qquad -1 \leqslant x \leqslant 1, \qquad t \geqslant 0, \end{aligned} \tag{24}$$

where the spatial discretization is accomplished by the fourth-order compact scheme described in detail by Eq. (11). The exact solution is

$$U(t, x) = \sin 2\pi(x - t), \qquad -1 \leqslant x \leqslant 1, \qquad t \geqslant 0. \tag{25}$$

A grid convergence study with boundary conditions of various orders is performed to show the formal accuracy of the resulting schemes. The boundary condition formulas expressed at the grid point $j = 0$ are

$$\frac{\partial V_0}{\partial x} + 3\frac{\partial V_1}{\partial x} = \frac{1}{6\,\Delta x}(-17V_0 + 9V_1 + 9V_2 - V_3) \tag{26}$$

$$\frac{\partial V_0}{\partial x} + 2\frac{\partial V_1}{\partial x} = \frac{1}{2\,\Delta x}(-5V_0 + 4V_1 + V_2) \tag{27}$$

$$\frac{\partial V_0}{\partial x} + \frac{\partial V_1}{\partial x} = \frac{1}{2\,\Delta x}(-V_0 + V_1) \tag{28}$$

$$\frac{\partial V_0}{\partial x} = \frac{1}{\Delta x}(-V_0 + V_1) \tag{29}$$

which represent fourth-, third-, second-, and first-order closures at the inflow boundary, respectively. As mentioned earlier, the physical boundary condition is imposed at the point $j = 0$, but actually occurs at the point $j = 1$. The closure could have been written explicitly for the point $j = 1$ by combining Eq. (30)

$$\frac{\partial V_0}{\partial x} + 4\frac{\partial V_1}{\partial x} + \frac{\partial V_2}{\partial x} = \frac{1}{\Delta x}(-3V_0 + 3V_2) \tag{30}$$

with Eqs. (26)–(29) to yield

$$\frac{\partial V_1}{\partial x}+\frac{\partial V_2}{\partial x}=\frac{1}{6\,\Delta x}(-V_0-9V_1+9V_2+V_3) \quad (31)$$

$$2\frac{\partial V_1}{\partial x}+\frac{\partial V_2}{\partial x}=\frac{1}{2\,\Delta x}(-V_0-4V_1+5V_2) \quad (32)$$

$$3\frac{\partial V_1}{\partial x}+\frac{\partial V_2}{\partial x}=\frac{1}{\Delta x}(-V_0-2V_1+3V_2) \quad (33)$$

$$4\frac{\partial V_1}{\partial x}+\frac{\partial V_2}{\partial x}=\frac{1}{\Delta x}(-2V_0-V_1+3V_2). \quad (34)$$

At the outflow boundary, closure was accomplished with the expressions

$$\frac{\partial V_N}{\partial x}+3\frac{\partial V_{N-1}}{\partial x}=-\frac{1}{6\,\Delta x}(-17V_N+9V_{N-1}+9V_{N-2}-V_{N-3}) \quad (35)$$

$$\frac{\partial V_N}{\partial x}+2\frac{\partial V_{N-1}}{\partial x}=-\frac{1}{2\,\Delta x}(-5V_N+4V_{N-1}+V_{N-2}) \quad (36)$$

$$\frac{\partial V_N}{\partial x}+\frac{\partial V_{N-1}}{\partial x}=-\frac{1}{2\,\Delta x}(-V_N+V_{N-1}) \quad (37)$$

$$\frac{\partial V_N}{\partial x}=-\frac{1}{\Delta x}(-V_N+V_{N-1}) \quad (38)$$

which represent fourth-, third-, second-, and first-order spatial accuracies, respectively. These expressions are valid for the point $j=N$ because no physical condition is imposed there.

In all cases, the temporal discretization was accomplished with the fourth-order R–K algorithm. At every iteration, the solution was advanced for the grid points $j=0$, N, followed by overwriting the boundary condition at the point $j=0$. Because the inflow boundary condition is a nonlinear function of time, the physical boundary condition must be applied at the proper intermediate level in time. Failure to do so degrades the formal accuracy of the method. The CFL used in the simulations was in the range $0.1 \leqslant \mathrm{CFL} \leqslant 1$, well within the Von Neumann stability condition for the Cauchy problem. The formal truncation of the method is $O(\Delta t^4)$; the error in time decays to the fourth power of the CFL for a given grid and can be made as small as desired by decreasing the CFL. Typically, CFLs $\leqslant 0.1$ were not needed because the dominant temporal terms in the modified equation were negligible compared with spatial terms. Further reduction of the CFL resulted in no change in the error of the scheme. This method was used in the sixth-order simulations to determine formal accuracy by decreasing the CFL further and ensuring that no temporal error remained in the solution. Finally, a third-order R–K was used to test the generality of the temporal discretization in several cases. The results were quantitatively similar.

An equivalent time $T=25$ was used in all simulations for all grids and methods at CFL = 0.25. The error at T was then calculated and reported as an L_2 norm. The L_∞ norm produced similar results, but it is not reported here. For methods that are Lax stable, the error is bounded uniformly at each stage for $0<\Delta t<\tau$ and $0 \leqslant k\,\Delta t \leqslant T$, where k is the number of time steps. If the grid at constant CFL is doubled, then the error should decrease at time level T by a factor $(\frac{1}{2})^p$, where p is the order of the method. The formal accuracy of each scheme was determined in this manner for each of the Lax-stable schemes.

Tables Ia, Ib, and Ic show the effects of boundary closure on the global accuracy of the fourth-order compact inner scheme. Shown are the closure orders at each boundary, the absolute log (L_2) error at a fixed time T for various grids, and the convergence rate between two successive grid densities. Three scenarios are studied: (1) equivalent but low-order closure at each boundary; (2) high-order inflow closure with low-order outflow closure; (3) low-order inflow closure with high-order outflow closure. The grid density ranges from 10 to 25 grid points/2π rad. Increased solution accuracy is achieved as the boundary accuracy is increased. No apparent benefit is achieved by closing only one boundary with high-order boundary conditions.

The theory of Gustafsson [3] predicts that boundary conditions of order $N-1$ must be imposed to retain Nth-order global accuracy. In all cases, the results in Tables I agree with the theory of Gustafsson. Specifically, first-order closure results in second-order accuracy, second-order closure results in third-order accuracy, third- and fourth-order closure result in fourth-order accuracy. Note that the convergence rates are bounded from above by the theoretical limit, but often they can be as much as one order less than the theoretical accuracy. In this study, the imposition of lower order boundary conditions at the outflow plane results in a greater degree of error than at the inflow plane. Although the characteristic is pointing out of the domain at the outflow boundary, the error is not swept immediately out of the domain as might be expected.

The formal stability of the numerical boundary conditions used in this example are now derived. The fourth-order compact scheme is Cauchy stable for CFL $\leqslant 1.63$. The stability of the inflow and outflow boundary conditions on the semi-infinite domain must be demonstrated. We begin by testing the outflow stability. The partial differential equation is

$$\frac{\partial U}{\partial t}-\frac{\partial U}{\partial x}=0, \qquad x \geqslant 0, \qquad t \geqslant 0. \quad (39)$$

No boundary condition is required in this problem, although an NBS is imposed at $x=0$. As was done on the

TABLES I

Comparative Study of Effects of Boundary Closure on Formal Accuracy for Fourth-Order Compact Inner Scheme

TABLE Ia

Equivalent Inflow and Outflow Accuracy

Inflow order	1st		2nd		3rd		4th	
Outflow order	1st		2nd		3rd		4th	
Grid	$\log(L_2)$	Rate	$\log(L_2)$	Rate	$\log(L_2)$	Rate	$\log(L_2)$	Rate
21	−0.831	NA	−2.803	NA	−2.046	NA	−2.835	NA
31	−1.289	−1.13	−3.499	−1.72	−3.291	−3.07	−4.758	−4.74
41	−1.636	−1.21	−4.023	−1.82	−4.179	−3.08	−5.965	−4.19
51	−1.914	−1.25	−4.448	−1.90	−4.868	−3.09	−6.760	−3.56

TABLE Ib

Fixed Fourth-Order Inflow with Variable Outflow Accuracy

Inflow order	4th		4th		4th		4th	
Outflow order	1st		2nd		3rd		4th	
Grid	$\log(L_2)$	Rate	$\log(L_2)$	Rate	$\log(L_2)$	Rate	$\log(L_2)$	Rate
21	1.230	NA	−0.932	NA	−1.864	NA	−2.835	NA
31	0.490	−1.83	−1.935	−2.47	−3.240	−3.39	−4.758	−4.74
41	0.031	−1.60	−2.587	−2.26	−4.176	−3.25	−5.965	−4.19
51	−0.252	−1.26	−3.087	−2.24	−4.858	−3.05	−6.760	−3.56

TABLE Ic

Variable Inflow and Fixed Fourth-Order Outflow Accuracy

Inflow order	1st		2nd		3rd		4th	
Outflow order	4th		4th		4th		4th	
Grid	$\log(L_2)$	Rate	$\log(L_2)$	Rate	$\log(L_2)$	Rate	$\log(L_2)$	Rate
21	−1.715	NA	−2.176	NA	−2.412	NA	−2.835	NA
31	−2.185	−1.16	−3.130	−2.35	−3.809	−3.44	−4.758	−4.74
41	−2.541	−1.23	−3.792	−2.30	−4.761	−3.31	−5.965	−4.19
51	−2.823	−1.26	−4.298	−2.27	−5.478	−3.21	−6.760	−3.56

Note. The test case was the equation $u_t + u_x = 0$ with sinusoidal inflow (all tables).

normal modal analysis for the finite domain, a solution of the form $V_j(t) = e^{St}\phi_j$ is assumed where $\phi_j = \phi_o \kappa^j$. Substitution into the inner scheme produces the resolvent condition for the eigenvalue $\hat{S}$,

$$\left(\frac{1}{\kappa} + 4 + \kappa\right)\hat{S} = 3\left(\frac{-1}{\kappa} + \kappa\right), \tag{40}$$

at each grid point where $j \geqslant 1$. At grid point $j = 0$, the scheme was closed with one of the boundary expressions given in Eqs. (26)–(29). Substitution of $V_j(t)$ into these expressions yields

$$(6 + 18\kappa)\,\hat{S} = -17 + 9\kappa + 9\kappa^2 - \kappa^3 \tag{41}$$

$$(2 + 4\kappa)\,\hat{S} = -5 + 4\kappa + \kappa^2 \tag{42}$$

$$(2 + 2\kappa)\,\hat{S} = -1 + \kappa \tag{43}$$

$$\hat{S} = -1 + \kappa. \tag{44}$$

Equation (40) is solved for $\hat{S}$ and substituted into Eqs. (41)–(44) to yield polynomials in κ of the form

$$(\kappa - 1)^5 = 0 \quad \text{(4th)} \tag{45}$$

$$(\kappa - 1)^4 = 0 \quad \text{(3rd)} \tag{46}$$

$$(\kappa - 1)^3 = 0 \quad \text{(2nd)} \tag{47}$$

$$(\kappa - 1)^2(\kappa + 2) = 0 \quad \text{(1st)}. \tag{48}$$

Clearly, the only value of κ that will simultaneously satisfy the inner resolvent condition and any of the outflow boundary conditions is $\kappa = 1$. Substitution of $\kappa = 1$ into the resolvent condition produces $\hat{S} = 0$, the case for which the perturbation test in G–K–S theory (condition V) must be used to show stability. Substitution of $\kappa = 1 - \varepsilon$ into the resolvent condition produces to first order

$$6\hat{S} = -6\varepsilon. \tag{49}$$

For $\varepsilon > 0$ and $|\kappa| < 1$, $\hat{S} < 0$ shows stability of the perturbation. All of the tested outflow boundary conditions are G–K–S stable; thus, $\kappa = 1$ is not a generalized eigenvalue.

To show stability of the inflow conditions, we study the partial differential equation

$$\frac{\partial U}{\partial t} + \frac{\partial U}{\partial x} = 0, \qquad x \geqslant 0, \qquad t \geqslant 0, \tag{50}$$

with the boundary condition imposed at $x = 0$ of the form

$$U(0, t) = g(t), \qquad t \geqslant 0. \tag{51}$$

Despite the physical boundary condition imposed at $j = 0$, an NBS must be imposed at $j = 1$ and must be tested for stability. Substitution of $V_j(t) = e^{St}\phi_j$ (where $\phi_j = \phi_o \kappa^j$) into the inner scheme produces the resolvent condition $(1/\kappa + 4 + \kappa)\,\hat{S} = -3(-1/\kappa + \kappa)$. Substitution into the first- through fourth-order boundary conditions defined by Eqs. (31)–(34) produces equations for $\hat{S}$ of the form

$$(6 + 6\kappa)\,\hat{S} = -9 + 9\kappa + \kappa^2 \tag{52}$$

$$(4 + 2\kappa)\,\hat{S} = -4 + 5\kappa \tag{53}$$

$$(3 + \kappa)\,\hat{S} = -2 + 3\kappa \tag{54}$$

$$(4 + \kappa)\,\hat{S} = -1 + 3\kappa. \tag{55}$$

Without loss of generality, we have assumed that $g(t)=0$ on the inflow boundary $j=0$, which eliminates the influence of $j=0$ in the boundary polynomial and reduces the order of the polynomials by one. The resolvent equation is solved for $\hat{S}$ and is substituted into Eqs. (52)–(55) to yield polynomials in κ of the form

$$(\kappa^4-5\kappa^3+10\kappa^2-9\kappa+9)=0 \quad \text{(4th)} \tag{56}$$

$$(\kappa^3-4\kappa^2+5\kappa-8)=0 \quad \text{(3rd)} \tag{57}$$

$$(\kappa^2-2\kappa+7)=0 \quad \text{(2nd)} \tag{58}$$

$$(\kappa^2-2\kappa-11)=0 \quad \text{(1st)}, \tag{59}$$

$$\tag{60}$$

the roots of which are

$$\kappa=2.286\pm 1.215i,\ 0.2134\pm 1.138i \quad \text{(4th)} \tag{61}$$

$$\kappa=3.218,\ 0.3906\pm 1.527i \quad \text{(3rd)} \tag{62}$$

$$\kappa=1\pm\sqrt{6}\,i \quad \text{(2nd)} \tag{63}$$

$$\kappa=1\pm 2\sqrt{3}\,i \quad \text{(1st)}, \tag{64}$$

where $i=\sqrt{-1}$. In all of these expressions $|\kappa|>1$. No eigenvalues or generalized eigenvalues exist, and the inflow boundary is stable for these closures. The fact that the Cauchy problem and the two quarter-plane problems are stable implies that the finite-domain problem defined in Eq. (11) is G–K–S stable for all boundary conditions specified thus far.

A more rigorous example of the ability of the G–K–S theory to predict the stability of the fourth-order compact scheme is demonstrated by a pathological inflow boundary scheme. Because the inflow problem involves an NBS at the grid point $j=1$, which is biased in the downwind direction, the scheme should be more sensitive to instability than the outflow boundary. A bounded scheme is formulated that is a linear combination of the first- and second-order schemes, both of which are stable boundary treatments. The resulting scheme that is used at the inflow boundary is

$$(1+2\beta)\frac{\partial V_0}{\partial x}+\frac{\partial V_1}{\partial x}=2(1+\beta)\frac{1}{\Delta x}(-V_0+V_1) \tag{65}$$

where β is the amount of the first-order influence in the formula. For $\beta=0$, the standard second-order closure is obtained. For all other values of β, the scheme is formally first-order accurate. This scheme is denoted as (1^1–4–4) because the inflow boundary is a one-parameter family of first-order schemes and the outflow is closed with a fourth-order formula. As was done previously, the dependence of the formula on the space derivative at $j=0$ is eliminated from Eq. (65) by the inner scheme written at $j=1$. The resulting expression is

$$\left[2(1+2\beta)-\frac{1}{2}\right]\frac{\partial V_1}{\partial x}+\frac{(1+2\beta)}{2}\frac{\partial V_2}{\partial x}$$
$$=\frac{1}{2\,\Delta x}\left[-(1+4\beta)\,V_0-2(1+\beta)\,V_1\right.$$
$$\left.+3(1+2\beta)\,V_2\right]. \tag{66}$$

Substitution of $V_j(t)=e^{St}\phi_j$, where $\phi_j=\phi_o\kappa^j$, into Eq. (66) (assuming $g(t)=0$) results in a boundary scheme of the form

$$\left[2(1+2\beta)-\frac{1}{2}\right]+\frac{(1+2\beta)}{2}\kappa\hat{S}$$
$$=-(1+\beta)+\frac{3}{2}(1+2\beta)\,\kappa. \tag{67}$$

If the inner scheme equation (40) is solved for $\hat{S}$ and substituted into Eq. (67), then a polynomial in κ results of the form

$$(-1+2\beta)\,\kappa^2+(2-4\beta)\,\kappa-(7+22\beta)=0. \tag{68}$$

Solving for κ yields

$$\kappa=1\pm\sqrt{6(4\beta+1)/(2\beta-1)}, \qquad \beta\neq\tfrac{1}{2}. \tag{69}$$

A double root exists for $\beta=-1/4$ and $\kappa=1$. Substitution of $\kappa=1$ into the resolvent expression yields $\hat{S}=0$; a perturbation test shows that the boundary exhibits a generalized eigenvalue instability. Further inspection of Eq. (69) shows that $|\kappa|\leqslant 1$ over the range $-5/8\leqslant\beta\leqslant-1/4$. All other values of β need not be considered as candidates for instability because $|\kappa|>1$. Substitution of the expression for κ obtained from Eq. (69) into Eq. (67) yields an expression for $\hat{S}$ in terms of the parameter β. Numerical evaluation of this expression shows that $\mathscr{R}(\hat{S})\geqslant 0$ for $-0.37\leqslant\beta\leqslant-1/4$. Thus, an eigensolution exists for this range, and the coupled inner boundary scheme is unstable.

To verify these findings, the model scalar wave equation described by Eqs. (23)–(25) was solved with the pathological inflow boundary conditions described in Eq. (65). Fourth-order boundary conditions were used at the outflow boundary. Figure 1 shows the results of the numerical investigation. Log_{10} of the L_2 error of the solution integrated to a fixed time T, as a function of the parameter β, ranging from $[\frac{-1}{2}, \frac{1}{2}]$, is plotted. The grid densities shown in the study behave similarly. The theoretically predicted range of instability $-0.37\leqslant\beta\leqslant-1/4$ is replicated in the numerical study to within graphical limitations of the plot.

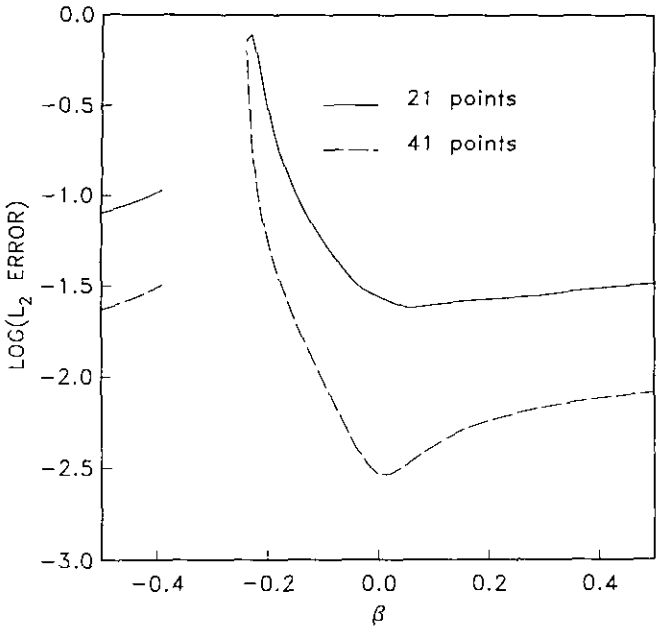

FIG. 1. Numerical determination of L_2 error at time level "T" from a one-parameter family of closure formulas at the inflow boundary (inner scheme is the fourth-order Padé scheme) with stable inflow conditions.

In the unstable regime, the error grew exponentially with the number of iterations required to reach the time level T and quickly became very large.

Although these boundary conditions are pathological, this study indicates that imposition of first-order inflow boundary conditions is not sufficient to guarantee stability with the fourth-order compact inner scheme. A similar experiment was performed on the outflow boundary with a linear combination of first- and second-order boundary conditions. For those boundary conditions, no eigensolutions could be found. Although this does not establish that any first-order outflow boundary condition is stable, it does indicate that the outflow is less susceptible to instabilities than the inflow boundary.

SEMIDISCRETE EIGENVALUE ANALYSIS

The uniformly fourth-order explicit scheme (4, 4–4–4, 4) analyzed by Strikwerda [8] and the uniformly fourth-order compact scheme (4–4–4) presented here are both G–K–S stable for the semidiscrete problem and, therefore, will exhibit generalized stability for the fully discrete problem if advanced with a locally stable temporal scheme. This definition of stability ensures that the error of the numerical solution will remain uniformly bounded for all times by an exponentially increasing amount. The exponential growth rate of the error is asymptotically independent of the grid used ($N \to \infty$, where N is the total number of grid points used). Thus, grid refinement studies with these methods, performed by integrating the governing equation to a fixed time level T on successively finer grids, will demonstrate that the numerical solution converges to the exact solution at a rate of at least the order of the method.

A disturbing feature of this stability definition is that the solution is not required to remain bounded for all times, even though the physical solution remains bounded for all times. Figure 2 shows a grid refinement study performed with the fourth-order compact (4–4–4) scheme to demonstrate this behavior. In the model equation was that described by Eqs. (23)–(25), the time interval was $0 \leqslant t \leqslant 100$ and the grids used were 21, 41, and 81 grid points, respectively. Time was advanced with a fourth-order R–K scheme in all cases. The exact solution is a traveling sine wave of amplitude one for all times. Shown is the $\log_{10}$ of the L_2 error, plotted as a function of time. Simulations on all three grids were run at various CFLs. The initial portion of the simulation is characterized by nearly constant levels of error on all three grids. After a sufficiently long time, the unstable modes in the numerical solution dominate the spatial truncation error. From that point on, the solution diverges exponentially from the exact solution. The growth rate in time of the unstable modes of the solution in nearly grid independent; at any time T, a refinement of the grid by a factor of 2 results in a decrease in the error by a factor of 16. At large times, the actual error will be exponentially large. An interesting feature of the numerical method is that the exponential growth of the solution is dependent upon the CFL used to advance the solution. For CFL = 1, the solution does not grow in time, but for CFL $\leqslant \alpha$ (α is some

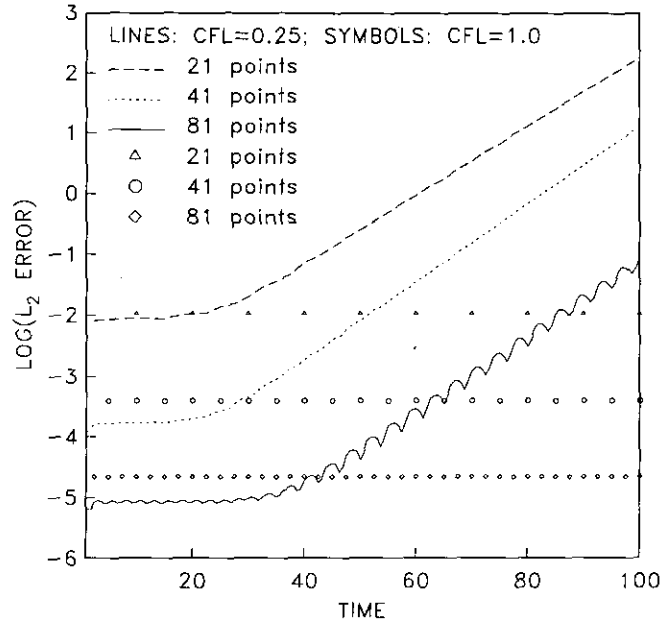

FIG. 2. The L_2 error as a function of time from uniformly fourth-order Padé scheme (4–4–4) for various CFLs and grid densities.

critical value less than CFL_{max}), exponential growth is observed. (This feature will be explained later in terms of the amplification factor of the scheme.) Regardless of the CFL, fourth-order convergence is observed with the scheme.

To understand the fundamental nature of the fixed-grid temporal divergence of the solution in the previous example, the eigenvalue spectrum of the spatial discretization operator is examined. As a semidiscretization, Eq. (23) can be written in the form of Eq. (5) as

$$\frac{dV}{dt} = MV + Bg(t), \tag{70}$$

where M is the $N \times N$ matrix that describes the spatial discretization operator and $Bg(t)$ represents the physical boundary data. Assume that

$$P^{-1}MP = S, \qquad P^{-1}U = V, \qquad P^{-1}Bg(t) = H, \tag{71}$$

where S is a diagonal matrix and P^{-1} and P are similarity transforms composed of the left and right eigenvectors of the matrix M, respectively. Equation (70) then takes the form

$$\frac{dU}{dt} = SU + H \tag{72}$$

The solution to Eq. (72) is

$$U_j(t) = e^{S_j t}U_j(0) + \int_0^t e^{S_j(t-\tau)}H_j(\tau)\,d\tau, \qquad j = 1, \ldots, N. \tag{73}$$

In this form, the solution to Eq. (72) depends exponentially on the eigenvalues S_j of the matrix M. This solution assumes that the eigenvalues S_j are not degenerate and $H(t)$ is not at a resonance frequency. If either of these situations occur, then the solution would include terms proportional to $t^p e^{S_j t}$, where p is the order of the degeneracy. The precise behavior depends on the temporal nature of $H(t)$, but for boundary data that remains bounded for all time, the solution generally grows only for the modes that have eigenvalues S_j with positive real parts. In addition, the growth rate will be governed by the eigenvalue with the largest positive component. Thus, any spatial discretization to the semidiscrete problem defined in Eq. (70) will exhibit exponential divergence of the solution from the bounded physical solution, if it has an eigenvalue in the right half of the complex plane (RH-P).

Figures 3 and 4 show the eigenvalue spectrum that results from the explicit fourth-order and the compact fourth-order spatial operators, which are closed at the boundaries with schemes of third- or fourth-order accuracy. In short-hand nomenclature, the explicit cases (3, 3–4–3, 3) and (4, 4–4–4, 4) are shown in Fig. 3, and the compact cases (3–4–3) and (4–4–4) are shown in Fig. 4. The spectrums are shown on grids of 21, 41, and 81 points, respectively. If the inner schemes are closed with third-order NBSs in both cases, then an eigenvalue spectrum results that is bounded

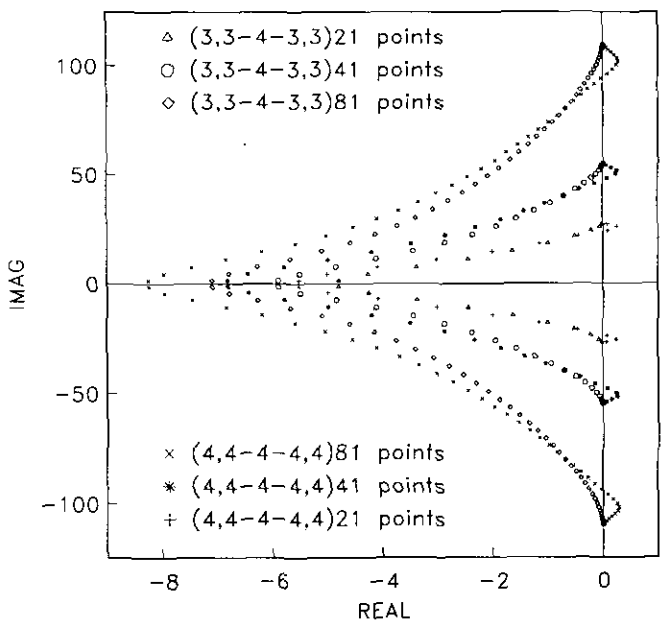

FIG. 3. Numerically determined eigenvalue spectrum from explicit fourth-order inner scheme, closed with either third- or fourth-order boundary schemes.

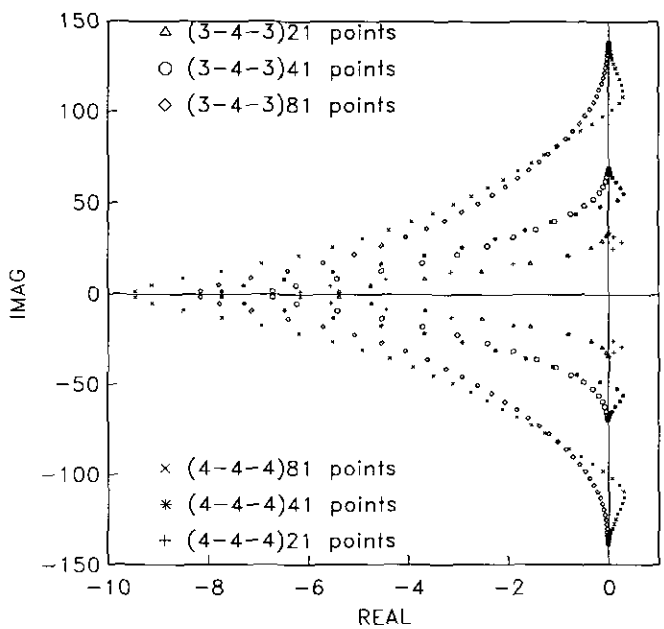

FIG. 4. Numerically determined eigenvalue spectrum from fourth-order Padé inner scheme, closed with either third- or fourth-order boundary schemes.

to the LH-P while the uniformly fourth-order schemes cross over the imaginary axis into the RH-P.

For long times, the maximum eigenvalues from the uniformly fourth-order schemes accurately predict the exponential growth of the solution. In Fig. 2, the solutions obtained from the (4–4–4) compact scheme grow exponentially in time. If the error can be represented functionally as $\varepsilon_N(t) = \varepsilon_N(0)\, e^{\alpha_N t}$ (where N is the number of grid points used in the spatial discretization), then a growth rate α_N can be determined numerically. From an eigenvalue determination, an effective growth rate α_S defined by $e^{\alpha_S N\, \Delta t} = |G_{\max}(\Delta t)|^N$ can be similarly calculated, where $G_{\max}$ is the numerical amplification obtained from the temporal advancement scheme. For the fourth-order R–K scheme,

$$G_j = 1 + S_j\, \Delta t + \frac{(S_j\, \Delta t^2)}{2!} + \frac{(S_j\, \Delta t^3)}{3!} + \frac{(S_j\, \Delta t^4)}{4!}, \qquad j = 1, \ldots, N, \tag{74}$$

and $|G_{\max}|$ will frequently correspond to the maximum eigenvalue $\mathscr{R}(S_{\max})$. Table II shows a comparison of the observed growth rate of the (4–4–4) compact scheme with the growth rate predicted from an eigenvalue determination. In each case, the maximum eigenvalue is used to predict the temporal growth of the solution. The agreement is very good, with a slight discrepancy for the 81-grid-point case. In Fig. 2, note the oscillatory growth of the solution. The uncertainty of the phase of the solution accounts for the discrepancy in the predicted growth rate in that case.

A necessary condition for Lax stability of the finite-domain semidiscretization can be expressed in terms of the eigenvalues of the spatial matrix operator as

$$\mathscr{R}(S_j) \leqslant \omega, \qquad \omega \geqslant 0, \qquad j = 1, \ldots, N, \tag{75}$$

where S_j are the eigenvalues of the spatial operator and N is an arbitrary number. The eigenvalue structure asymptotically approaches a bound in the RH-P as $N \to \infty$. All the fourth-order schemes presented thus far have satisfied this constraint. For the third-order NBSs (3, 3–4–3, 3) and (3–4–3), the constant is $\alpha = 0$; for the fourth-order NBSs, the constant is greater than zero.

As mentioned earlier, a curious feature of the (4–4–4) (as well as other high-order spatial schemes) is that the growth of the solution is CFL dependent on all grids. For CFLs close to the $\mathrm{CFL}_{\max}$, as determined from Von Neumann stability analysis, the schemes are bounded in time. For sufficiently small CFLs, the schemes begin to diverge exponentially in time. (In either case, the scheme is still G–K–S or Lax stable.) This behavior can be explained by noting a particular feature of the fourth-order R–K time-advancement scheme, as well as some of the other locally stable time schemes. The stability bound of a time-advancement scheme is defined as the locus of points in the complex plane where $|z| \leqslant 1$. Clearly, $|z| = 1$ divides the plane into two regions. When the spatial eigenvalues (scaled by Δt) of a particular discretization lie entirely within the $|z| = 1$ boundary, the combined time-space scheme is generally stable. The stability regime of these schemes includes a semicircular portion of the complex plane that is centered at the origin, is symmetric about the real axis, and extends into the LH-P. In addition, the stability regimes contain a small part of the RH-P, although not near the origin. If the spatial eigenvalues that lie in the RH-P are encompassed by the $|z| = 1$ boundary, then the resulting scheme is stable. If a Δt is chosen such that the $|z| = 1$ line does not contain the RH-P eigenvalues, then the solution diverges with time. Figure 5 shows this feature for the (4–4–4) spatial scheme and the fourth-order R–K scheme in time. For CFLs near the $\mathrm{CFL}_{\max}$, the maximum amplification rate $|G_{\max}|$ is less than one. For sufficiently small CFLs, the $|G_{\max}|$ is greater than one by an amount that is proportional to $\mathscr{R}(S_{\max})$, and the solution will diverge exponentially in time. A spatial scheme that has RH-P eigenvalues can always be made to diverge

TABLE II

Numerical versus Theoretical Growth Rate (4–4–4)

Grid	$\alpha_{\text{Numerical}}$	$\alpha_{\mathscr{R}(S_{\max})}$
21	0.1321	0.1315
41	0.1476	0.1474
81	0.1537	0.1479

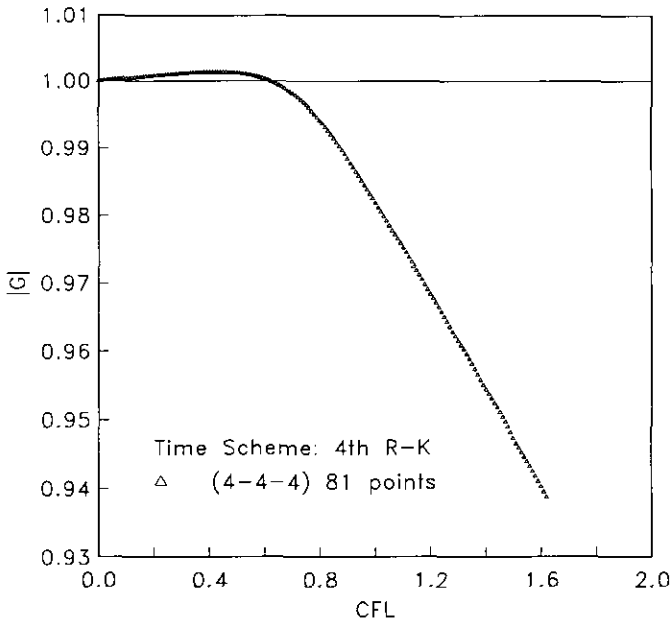

FIG. 5. Maximum numerical amplification factor as a function of CFL, plotted for uniformly fourth-order Padé scheme with a fourth-order R–K time-advancement scheme.

exponentially for sufficiently small CFLs, if a conventional third- or fourth-order R–K time-advancement scheme is used.

ASYMPTOTIC STABILITY

The previous discussion of Figs. 2 through 5 brings out a subtle point in the Lax stability theory. Different limit processes can be considered with numerical integration of time-dependent partial differential equations. One limit is the behavior of the numerical solution as the mesh size $\Delta x \to 0$ for a fixed time T. Another is the behavior of the solution for a fixed mesh as the time T tends to infinity.

Lax stability addresses the first issue, which is the boundedness of the numerical solutions as the mesh is refined at a fixed physical time. The Lax equivalence theorem states that if the numerical solution is bounded in this sense, then it converges to the true solution in the limit $\Delta x \to 0$. To obtain an approximation to the true solution at time T, the IBVP is integrated up to time T on a sequence of grids as $\Delta x \to 0$. This sequence converges to the exact solution for all time levels T.

Nothing in this definition excludes growth in time; the definition specifically allows exponential growth in time. Moreover, if each of the quarter-plane problems is stable and allows no growth in time, then the combined finite interval problem still allows exponential growth in time. (The Laplace transforms used in the G–K–S theory are legitimate only if growth in time is allowed.)

Unfortunately, for genuinely time dependent problems, this stability definition might be too weak, particularly if simulations are performed for long physical times. In order to achieve any reasonable accuracy for large times an excessive number of grid points are needed. For long time numerical simulations to be useful, the solution of the semidiscrete problem defined in Eq. (5) must be bounded in time as well. So, for a fixed mesh N, the eigenvalues of the matrix M in Eq. (5) have nonpositive real part, and those with zero real part have a geometrical multiplicity of one. This is called *asymptotic stability*.

By itself, asymptotic stability does not imply Lax stability. Numerous examples can be found in the literature of fully discrete schemes that are symptotically stable, but not Lax stable. The classic example is the case of a first-order upwind spatial operator that is advanced with an Euler explicit time-advancement scheme. The eigenvalues for the fully discrete system are $(1-\lambda)$ and occur a degenerate N times. Eigenvalue determination suggests that the CFL of the scheme should be two; however, Von Neumann analysis and practical experience suggest that a CFL of one is the maximum stable CFL. The discrepancy can be explained by the fact that for $1 < \text{CFL} < 2$, the matrix norm first grows rapidly and then decays asymptotically to zero. This difficulty might have been suspected by noting that, in the semidiscrete case, the degenerate eigenvalues allow geometric growth in time and only later are dominated by the exponentially decaying terms in the expressions.

An example for the semidiscrete case is now presented. Consider Eq. (5) with $g(t) = 0$. Let the matrix M be defined by the second-order central-difference operator for the interior points. In matrix form, M can be written as

$$M = \frac{1}{2}\begin{bmatrix} -1 & 1 & & & & & \\ -1 & 0 & 1 & & & 0 & \\ & \ddots & \ddots & \ddots & & & \\ & & & \ddots & \ddots & & \\ & 0 & & -1 & 0 & 1 & \\ & & & & -1 & 1 & \end{bmatrix}, \tag{76}$$

where the boundary closures at grid points $j = 1$ and $j = N$ are artificially chosen. With semidiscrete modal analysis, we determine a solution to Eq. (5) by assuming the form $V_j(t) = e^{St}\phi_j$ with $\phi = A\kappa^j + B(-1/\kappa)^j$. The resolvent condition from the interior scheme yields $S_j = \frac{1}{2}(\kappa - 1/\kappa)$. The boundary conditions are used at point $j = 1$ and $j = N$ to determine the values of A and B which yield the expression for κ of the form

$$(\kappa + 1)[(-1)^N - \kappa^{2N}] = 0. \tag{77}$$

The roots to Eq. (77) are $\kappa = -1$ and $\kappa = ie^{i\pi j/N}$ for $j = 1, N-1$. Thus, the eigenvalues are $S = 0$ and $S = i\cos(\pi j/N)$ for $j = 1, N-1$, and are purely imaginary. For values of N which are odd, the spatial discretization satisfies our definition as asymptotic stability.

The spatial discretization defined by Eq. (76) admits a generalized eigenvalue instability at the inflow boundary. The use of G–K–S analysis for the inflow boundary produces compatibility equations of the form

$$\begin{aligned} 2\hat{S}\kappa &= \kappa - 1, \qquad j = 1, \\ 2\hat{S}\kappa^2 &= \kappa^3 - \kappa, \qquad j = 2, \end{aligned} \tag{78}$$

for which the only solution is $\kappa = 1$, $\hat{S} = 0$. The boundary condition is unstable to perturbations away from the unit circle and, therefore, exhibits a generalized eigenvalue instability at the boundary. Asymptotic stability for the semidiscrete problem does not guarantee Lax stability.

Additionally, Reddy and Trefethen [15] have shown that consideration of the exact eigenvalues is not sufficient to determine the stability of a method. The famous Kreiss matrix theorem gives necessary and sufficient conditions for Lax stability in terms of the eigenvalues of the matrix M. A useful and equivalent test for determining stability is the analysis of the resolvent condition, which is interpreted by Reddy and Trefethen to involve not only the eigenvalues of the matrix M, but also to involve the ε pseudospectrum of

the discretization matrix. This pseudospectrum is obtained by perturbing the matrix M by an arbitrary matrix of norm ε. Examples of where the ε pseudoeigenvalues determine the stability bounds of numerical methods are given by Reddy *et al.* [15].

A stability definition based on the eigenvalue determination of the spatial operator is not sufficient to guarantee stability. (No attempt has been made to address the variable coefficient, nonlinear scalar cases, or the hyperbolic system. It is unlikely that the definition will generalize to all these situations.) However, for the present applications of higher order schemes, a restriction of the allowable numerical discretizations to those that possess Lax stability and the property of bounded LH-P eigenvalues is useful. For a broad class of spatial discretizations, these constraints are sufficient for the stability of the resulting numerical scheme and will be pursued in the remainder of this work.

Before this discussion on fourth-order spatial discretizations is completed, a uniformly fourth-order scheme should be devised. We know that conventional discretization formulas at the boundaries result in G–K–S stable, but not asymptotically stable, schemes for both the explicit and compact cases. The NBSs used in each case relied on optimal order schemes at the boundary, where $N+1$ constraints were used to devise the Nth-order scheme. By removing the constraint of using optimal schemes at the boundaries, an NBS with different dissipative characteristics can be devised and an asymptotically stable spatial scheme can be found that is uniformly fourth-order.

An asymptotically stable fourth-order compact scheme is devised first, which we shall denote as $(4^3\text{–}4\text{–}4^3)$. The 4^3 signifies that the boundary point is closed with a fourth-order three-parameter family of schemes. The scheme defined at grid point $j=0$ can be written as

$$\frac{\partial U_0}{\partial x}=\frac{1}{\Delta x}\left(C_0U_0+C_1U_1+C_2U_2+C_3U_3+C_4U_4+C_5U_5+C_6U_6+C_7U_7\right). \tag{79}$$

To be formally fourth-order accurate, Taylor series truncation analysis relates the coefficients as

$$\begin{aligned}
C_0&=-(\alpha-28\beta+322\gamma+13068)/5040\\
C_1&=+(\alpha-27\beta+295\gamma+5040)/720\\
C_2&=-(\alpha-26\beta+270\gamma+2520)/240\\
C_3&=+(\alpha-25\beta+247\gamma+1680)/144\\
C_4&=-(\alpha-24\beta+226\gamma+1260)/144\\
C_5&=+(\alpha-23\beta+207\gamma+1008)/240\\
C_6&=-(\alpha-22\beta+190\gamma+840)/720\\
C_7&=+(\alpha-21\beta+175\gamma+720)/5040,
\end{aligned} \tag{80}$$

with similar expressions defined for the closure at the other end of the domain. By systematically searching the three-parameter space spanned by the parameters α, β, and γ, coefficients can be obtained to yield an eigenvalue spectrum that is bounded to the LH-P. The values of α, β, and γ are not unique, and no attempt was made to optimize the spectrum. A particular set of coefficients that makes the scheme asymptotically stable are $\alpha=-1560$, $\beta=-355$, and $\gamma=-35$. Figure 6 shows the resulting spectrum from the (2–4–2), (3–4–3), and $(4^3\text{–}4\text{–}4^3)$ schemes. In all cases the eigenvalues are bounded to the LH-P, and the resulting scheme is asymptotically stable.

Because the asymptotic stability condition $\mathscr{R}(S_j)\leqslant\omega$ for $\omega=0$ is a very strong, necessary condition, but is not a sufficient condition, G–K–S stability will still be shown for this case. For the outflow problem, the model equation is

$$\frac{\partial U}{\partial t}-\frac{\partial U}{\partial x}=0, \qquad x\geqslant 0, \qquad t\geqslant 0. \tag{81}$$

No boundary condition is required in this problem, although an NBS is imposed at $x=0$. If a solution of the form $V_j(t)=e^{St}\phi_j$ is assumed where $\phi_j=\phi_o\kappa^j$, then substitution into the inner scheme produces the resolvent condition for the eigenvalue $\hat{S}$,

$$\left(\frac{1}{\kappa}+4+\kappa\right)\hat{S}=3\left(\frac{-1}{\kappa}+\kappa\right) \tag{82}$$

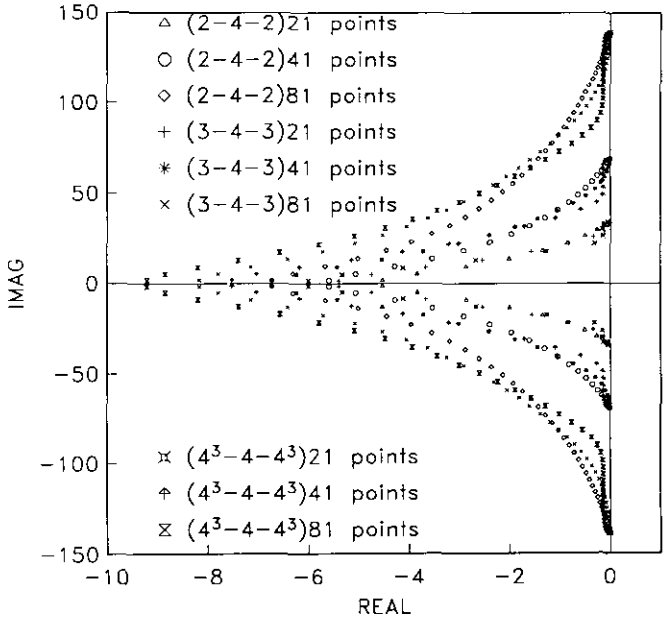

FIG. 6. Numerically determined eigenvalue spectrum from the fourth-order Padé inner scheme, closed with either second-, third-, or newly developed fourth-order boundary schemes.

at each grid point where $j \geqslant 1$. At grid point $j=0$, the parameter scheme produces an equation of the form

$$360\hat{S} = -(+727 - 1370\kappa + 1110\kappa^2 - 875\kappa^3 + 775\kappa^4 - 552\kappa^5 + 220\kappa^6 - 35\kappa^7). \quad (83)$$

The resolvent condition for $\hat{S}$ is solved and substituted into the boundary scheme to yield a polynomial in κ of the form

$$(\kappa - 1)^5 (35\kappa^4 + 95\kappa^3 - 168\kappa^2 - 227\kappa - 353) = 0. \quad (84)$$

When the polynomial is solved for κ, no roots are produced that are less than one in magnitude; thus, a stable condition results. The possibility that $\kappa = 1$ exists and must be checked for generalized eigenvalues. This condition is the same condition that was tested for outflow stability in Eq. (49), which was shown to be stable. Thus, the parametric fourth-order outflow scheme is G–K–S stable for the parameters α, β, and γ presented above.

To show stability of the parameter scheme at the inflow, we study the partial differential equation

$$\frac{\partial U}{\partial t} + \frac{\partial U}{\partial x} = 0, \qquad x \geqslant 0, \qquad t \geqslant 0, \quad (85)$$

with the boundary condition imposed at $x = 0$ of the form

$$U(0, t) = g(t), \qquad t \geqslant 0. \quad (86)$$

Elimination of $\partial U_0/\partial x$ between the boundary scheme at $j=0$ and the inner scheme at $j=1$ yields a combination boundary scheme of the form

$$1440\frac{\partial U_1}{\partial x} + 360\frac{\partial U_2}{\partial x} = -\frac{1}{\Delta x}(353U_0 + 1370U_1 - 2190U_2 + 875U_3 - 775U_4 + 552U_5 - 220U_6 + 35U_7). \quad (87)$$

Substitution of $V_j(t) = e^{St}\phi_o \kappa^j$ into the inner scheme and boundary schemes produces the resolvent condition equation (40) and

$$(1440\kappa + 360\kappa^2)\hat{S} = (+353U_0 + 1370\kappa^1 - 2190\kappa^2 + 875\kappa^3 - 775\kappa^4 + 552\kappa^5 - 220\kappa^6 + 35\kappa^7). \quad (88)$$

Equation (40) is solved for $\hat{S}$ and substituted into Eq. (88), together with the condition that $U_0 = 0$ yields a polynomial in κ of the form

$$\kappa(-2950 + 2210\kappa^1 - 2195\kappa^2 + 1615\kappa^3 - 1673\kappa^4 + 1213\kappa^5 - 293\kappa^6 - 80\kappa^7 + 35\kappa^8) = 0. \quad (89)$$

No roots for which $|\kappa| < 1$ result when this polynomial is solved. The only possibility for instability is the condition $|\kappa| = 1$. Again, this condition was checked previously for the other fourth-order schemes and was shown to be stable for the inflow. The compact three-parameter family (4^3–4–4^3) is stable for inflow and outflow when the parameters are $\alpha = -1560$, $\beta = -355$, and $\gamma = -35$. In addition, the scheme produces an eigenvalue spectrum for the scalar wave equation that is bounded to the LH-P. When the inflow and outflow boundaries of the explicit fourth-order scheme are treated in a similar manner (4^3, 4–4–4, 4^3), an asymptotically stable scheme is also produced. The resulting scheme was not tested for G–K–S stability in this work.

SIXTH-ORDER SCHEMES

As a last step in this work, the ideas and techniques used to analyze the fourth-order compact schemes are applied to sixth-order compact schemes. All the schemes tested here are based on the sixth-order, compact inner scheme developed by Lele [16]. The scheme is written as

$$\frac{\partial U_{j-1}}{\partial x} + 3\frac{\partial U_j}{\partial x} + \frac{\partial U_{j+1}}{\partial x} = \frac{1}{12\,\Delta x}(-U_{j-2} - 28U_{j-1} + 28U_{j+1} + U_{j+2}), \qquad j = 2, \ldots, N-2. \quad (90)$$

The scheme utilizes information from five points explicitly and three points implicitly. As a consequence of the five-point width of the stencil, NBSs must be provided at two points at each end of the domain: $j = 0$, 1 and $j = N-1$, N. The physical boundary condition is used at one of the inflow points. To ensure formal sixth-order accuracy for the hyperbolic problem, the boundary points must be closed with at least fifth-order formulas; for the optimal schemes, the shorthand nomenclature would be (5, 5–6–5, 5). In keeping with the convention of this work, the closure at each end of the domain is done in an asymmetric manner so that either the inflow or the outflow problem can be easily accommodated.

Formally sixth-order accurate G–K–S stable schemes are difficult to find. Therefore, the discussion begins with the stability analysis of a family of lower order schemes. Two of the schemes in this family are the (3, 5–6–5, 3) and

(4, 5–6–5, 4). The formal accuracies of these schemes are fourth and fifth order, respectively. The closure at the grid point $j=0$ (with corresponding formulas written at $j=N$) is accomplished by using

$$\frac{\partial U_0}{\partial x}+2\frac{\partial U_1}{\partial x}=\frac{1}{2\,\Delta x}(-5U_0+4U_1+U_2) \tag{91}$$

$$\frac{\partial U_0}{\partial x}+3\frac{\partial U_1}{\partial x}=\frac{1}{6\,\Delta x}(-17U_0+9U_1+9U_2-U_3) \tag{92}$$

for the third- and fourth-order schemes, respectively; the fifth-order closure at the point next to the wall is accomplished in all cases by the scheme

$$\frac{\partial U_0}{\partial x}+6\frac{\partial U_1}{\partial x}+3\frac{\partial U_2}{\partial x}=\frac{1}{3\,\Delta x}(-10U_0-9U_1+18U_2+U_3). \tag{93}$$

Wider spatial stencils produce stability polynomials of dramatically increased complexity. Despite the fact that MACSYMA was used to determine all of the spatial formulas and the stability polynomial of the sixth-order schemes, the possibility for error still exists. With the ability of the G–K–S theory to accurately predict the stability envelope of the one-parameter family of fourth-order compact schemes (1^1–4–4), a simple test was devised to verify the accuracy of the G–K–S calculations. A one-parameter family of schemes was created by combining the third- and fourth-order closure formula at each end of the domain. Symbolically, the combined scheme is represented by (3^1, 5–6–5, 3^1) and is written as

$$\alpha\left[\frac{\partial U_0}{\partial x}+2\frac{\partial U_1}{\partial x}-\frac{1}{2\,\Delta x}(-5U_0+4U_1+U_2)\right]+(1-\alpha)\left[\frac{\partial U_0}{\partial x}+3\frac{\partial U_1}{\partial x}-\frac{1}{6\,\Delta x}\times(-17U_0+9U_1+9U_2-U_3)\right]=0. \tag{94}$$

For $\alpha=0$ (or 1), the scheme produces the optimal fourth-order (or third-order) variant; for all other values of α, the formula is a third-order scheme.

The model equation for the outflow quarter-plane problem is the same as described in Eq. (81). Solutions of the form $U_j(t)=e^{St}\phi_0\kappa^j$ satisfy the numerical scheme and give the sixth-order inner scheme the resolvent condition

$$\left(\frac{1}{\kappa}+3+\kappa\right)\hat{S}=\left(-\frac{1}{\kappa^2}-\frac{28}{\kappa}+28\kappa+\kappa^2\right)\Big/12 \tag{95}$$

for the eigenvalue $\hat{S}$. In general, only two roots of the resolvent equation will yield $|\kappa|<1$ for a polynomial of degree four. The other two roots will become exponentially unbounded as j becomes large and can be ignored. The general solution has the form $U_j(t)=e^{St}(C_1\kappa_1^j+C_2\kappa_2^j)$. Substitution of this expression into the boundary equations (93) and (94) yields expressions for the constants C_1 and C_2:

$$\begin{aligned}C_1F_0(\kappa_1)+C_2F_0(\kappa_2)&=0\\ C_1F_1(\kappa_1)+C_2F_1(\kappa_2)&=0,\end{aligned} \tag{96}$$

where

$$\begin{aligned}F_0(\kappa)&=[-(6\alpha+18)\kappa-18\kappa^2]\hat{S}-[(2\alpha+3)+(3\alpha+27)\kappa\\&\quad-(6\alpha+27)\kappa^2+(\alpha-3)\kappa^3]\\ F_1(\kappa)&=[(1+6\kappa+3\kappa^2)\hat{S}-(-10-9\kappa+18\kappa^2+1\kappa^3)/3].\end{aligned} \tag{97}$$

Equation (96) has only the trivial solution unless the determinant condition is satisfied $(F_0(\kappa_1)F_1\kappa_2)-F_1(\kappa_2)F_0(\kappa_1)=0)$. When the resolvent equation (95) is solved for $\hat{S}$ and substituted into the determinant condition, an expression that relates the two κ's results:

$$(\kappa_1-1)^3(\kappa_2-1)^3[(7\alpha-3)\kappa_1\kappa_2+(-2\alpha+3)\times(\kappa_1+\kappa_2)-3\alpha-3]=0. \tag{98}$$

The solution to Eq. (98) yields $\kappa_1=1$, $\kappa_2=1$, or

$$\kappa_1=\frac{(2\alpha-3)\kappa_2+3\alpha+3}{(7\alpha-3)\kappa_2-2\alpha+3}. \tag{99}$$

To obtain an additional independent relationship for κ_1 and κ_2, the resolvent condition equation (95) is used. The resolvent equation is solved for $\hat{S}$ (note that both κ_1 and κ_2 satisfy this expression for $\hat{S}$) to yield

$$\hat{S}=\frac{(-1/\kappa_1^2-28/\kappa_1+28\kappa_1+\kappa_1^2)}{12(1/\kappa_1+3+\kappa_1)}=\frac{(-1/\kappa_2^2-28/\kappa_2+28\kappa_2+\kappa_2^2)}{12(1/\kappa_2+3+\kappa_2)}. \tag{100}$$

A combination of Eqs. (99) and (100) produces a single, sixth-order polynomial in κ_2, for which the roots can be found numerically. Equations (99) and (95) are then used to determine the numerical values of κ_1 and $\hat{S}$. An eigensolution exists for the problem if, for $|\kappa_1|<1$ and $|\kappa_2|<1$, an $\hat{S}$ exists with real part greater than zero.

If the outflow polynomial is solved for κ_2, then the boundary is unstable for $-9.16<\alpha<-1.86$. The two limiting cases ($\alpha=0$ and $\alpha=1$) for which the scheme is

fourth- or third-order accurate are stable. The possibility of instability also exists for the cases where $\kappa_1 = \kappa_2$ and κ_1 or $\kappa_2 = 1$. However, none of these conditions showed eigenvalue instability.

The model equation for the inflow quarter-plane problem is the same as that described in Eqs. (85) and (86). Solutions of the form $U_j(t) = e^{St}\phi_0\kappa^j$, will satisfy the numerical scheme to give the sixth-order inner scheme the resolvent condition

$$12\left(\frac{1}{\kappa}+3+\kappa\right)\hat{S} = -\left(-\frac{1}{\kappa^2}-\frac{28}{\kappa}+28\kappa+\kappa^2\right). \quad (101)$$

Elimination $\partial U_0/\partial x$ between the boundary schemes at grid points $j=0$ and $j=1$, yields an expression written for grid point $j=1$ of the form

$$(6\alpha+18)\frac{\partial U_1}{\partial x}+18\frac{\partial U_2}{\partial x} = \frac{1}{6\,\Delta x}[(2\alpha+3)\,U_0+(3\alpha+27)\,U_1 - (6\alpha+27)\,U_1+(\alpha-3)\,U_3]. \quad (102)$$

The general solution has the form $U_j(t) = e^{St}(C_1\kappa_1^j + C_2\kappa_2^j)$. Substitution of this expression into the boundary expressions at $j=1, 2$ yields two expressions for the constants C_1 and C_2,

$$\begin{aligned} C_1F_1(\kappa_1)+C_2F_1(\kappa_2) &= 0 \\ C_1F_2(\kappa_1)+C_2F_2(\kappa_2) &= 0, \end{aligned} \quad (103)$$

where

$$\begin{aligned} F_1(\kappa) &= [-(6\alpha+18)\,\kappa-18\kappa^2]\,\hat{S}-[+(3\alpha+27)\,\kappa \\ &\quad -(6\alpha+27)\,\kappa^2+(\alpha-3)\,\kappa^3] \\ F_2(\kappa) &= 1. \end{aligned} \quad (104)$$

The simple form of the expression $F_2 = 1$ results from reducing the modal equation at point $j=2$ (with U_0 set to zero) by use of the resolvent condition (with U_0 not equal to zero). Equations (103) can only have a nontrivial solution if the determinants are identically zero. Equation (101) is solved for $\hat{S}$ and substituted into the determinant condition from Eqs. (103) to yield

$$\frac{\left((2\alpha-3)\,\kappa_1^5+(-5\alpha+15)\,\kappa_1^4-30\kappa_1^3+(6\alpha+24)\,\kappa_1^2 + (-22\alpha-33)\,\kappa_1^1-(\alpha+3)\right)}{2\kappa_1^2+6\kappa_1^1+2} - \frac{\left((2\alpha-3)\,\kappa_2^5+(-5\alpha+15)\,\kappa_2^4-30\kappa_2^3+(6\alpha+24)\,\kappa_2^2 + (-22\alpha-33)\,\kappa_2^1-(\alpha+3)\right)}{2\kappa_2^2+6\kappa_2^1+2} = 0. \quad (105)$$

Together, Eqs. (100) and (105) provide two equations for the unknown κ_1 and κ_2.

The inflow polynomial equations are far more difficult to solve because they do not factor appreciably. A change of variables from κ_1 and κ_2 to x and y simplifies the algebra. Substitution of

$$\begin{aligned} \kappa_1+\kappa_2 &= 2y \\ \kappa_1\kappa_2 &= x \end{aligned} \quad (106)$$

into Eq. (100) yields

$$(-8x-8)\,y^2+(-12x^2-224x-12)\,y - 2x^3-166x^2-166x-2=0 \quad (107)$$

which has the solution

$$y = \frac{-(3x^3+56x+3\pm\sqrt{5x^4+2490x^2+5})}{4x+4} \quad (108)$$

for $x \neq -1$. (The case $x=-1$ degenerates into $y=0$ for which $\kappa_1 = -\kappa_2 = \pm 1$, a condition that produces no eigensolutions). Either root can be used because the final polynomial results from the square of an intermediate result (to clear the square root in the expression). Equation (106) is substituted into Eq. (105) and, further, is simplified with the expression for y from Eq. (108) to yield a ninth-order polynomial in the variable x, with coefficients that are functions of the variable α. This expression is solved numerically to yield the roots for x. The values of y are then determined

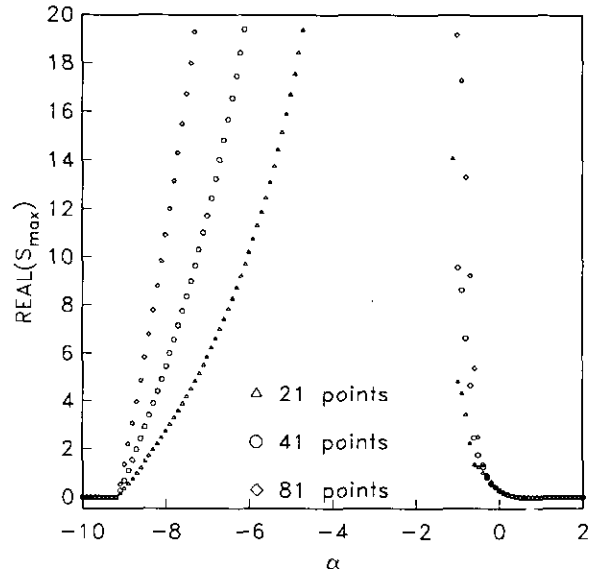

FIG. 7. Maximum real part of the numerically determined eigenvalue spectrum (3^1, 5–6–5, 3^1) from a sixth-order Padé inner scheme and a one-parameter family (in α) of third-order boundary schemes.

from Eq. (108), and the values of κ_1 and κ_2 are obtained from Eq. (106). Again, the condition $\kappa = 1$ and the case where $\kappa_1 = \kappa_2$ did not show instability over the parameter range tested in this study. For the inflow boundary condition, the instability envelope for the parameter α was determined to be $-1.86 \leqslant \alpha \leqslant -0.447$. The two degenerate conditions, $\alpha = 0$ and $\alpha = 1$, are G–K–S stable for the inflow. By combining the inflow and outflow results, the theoretical (G–K–S) range of instability for the one-parameter family of schemes (3^1, 5–6–5, 3^1) was determined to be $-9.18 \leqslant \alpha \leqslant -0.447$. The two degenerate cases, (3, 5–6–5, 3) and (4, 5–6–5, 4), were both G–K–S stable schemes.

To determine the accuracy of the G–K–S calculations, another method of showing stability was used and the results were compared. The necessary condition for stability on the eigenvalue structure $\mathscr{R}(S_{\max})$ provides such a test. Figure 7 shows the results of an eigenvalue determination that spans the range $-10 \leqslant \alpha \leqslant 2$, as determined numerically. The maximum eigenvalue $\mathscr{R}(S_{\max})$ (the eigenvalue with the largest absolute real component) is plotted as a function of the parameter α for three grid densities. Because Lax stability in a finite domain requires that $\mathscr{R}(S) \leqslant \omega$ for $\omega \geqslant 0$, the $\mathscr{R}(S_{\max})$ should remain bounded with increasing grid density if the scheme is to be stable for a particular value of α. Figure 7 shows that the stability boundary at $\alpha = -9.15$ is accurately predicted by G–K–S theory. The stability boundary at $\alpha = -0.45$ is less well defined in the eigenvalue determination and must be further investigated to show the correlation between G–K–S theory and eigenvalue determination. On the relatively coarse grids presented in Fig. 7, the maximum eigenvalues near the limit $\alpha = -0.45$ grow as grid density increases. Whether they grow in a bounded manner determines if they satisfy the necessary condition for stability. Table III shows the behavior of $\mathscr{R}(S_{\max})$ for various grid densities at $\alpha = -0.4$.

As the number of grid points becomes larger, the maximum eigenvalue asymptotes to a constant ω; thus, a stable condition results. Note that the convergence to the asymptotic limit is slow for $\alpha = -0.4$. Similar grid refinement studies at values of $\alpha = -0.45$ and -0.5 showed linear growth for all grids, which resulted in an unstable condition. Based on a numerically determined eigenvalue determination over the range of $-10 \leqslant \alpha \leqslant 2$, the G–K–S theory accurately predicts the stability envelope. The slow convergence to the asymptotic determination a somewhat unreliable method for determining stability. However, for many nonborderline cases, it does provide an accurate measure of stability.

The eigenvalue determination provides information on the asymptotic stability of the schemes as well. If the $\mathscr{R}(S_{\max}) \leqslant 0$ for all the grids, then the scheme is asymptotically stable. For values of the parameter $\alpha \leqslant -9.15$ and $\alpha \geqslant 0.4$, eigenvalue determination indicates the asymptotic as well as the Lax stability of the resulting scheme. Figure 8 shows the eigenvalue spectrum of the (3, 5–6–5, 3) and (4, 5–6–5, 4) schemes. Both schemes satisfy the necessary condition of Lax stability; the (3, 5–6–5, 3) scheme is asymptotically stable. Because of the eigenvalues in the RH-P, the (4, 5–6–5, 4) scheme does not exhibit asymptotic stability. Figure 9 shows a plot of the error of the solution to the scalar wave equation defined by Eqs. (23)–(25) when discretized with the (4, 5–6–5, 4) scheme. The time interval was $0 \leqslant t \leqslant 100$, and time was advanced with a fourth-order R–K scheme. The $\log_{10}$ of the L_2 error is plotted as a function of time for grid densities of 21, 41, and 81 points, respectively. For a CFL = 1, the error does not grow in time. For CFLs of order 0.1, the error is nearly uniform for a period of time; then it grows exponentially with time. In all cases, the error of the simulation decreases by a factor of 16 to 32 when the grid is doubled. (Error is dominated by

TABLE III

Grid Convergence of $\mathscr{R}(S_{\max})$ for $\alpha = -0.4$

Grid	$\mathscr{R}(S_{\max})$	Δ%
21	1.000	NA
41	1.250	25
81	1.360	8
161	1.582	16
321	1.704	8
641	1.780	5

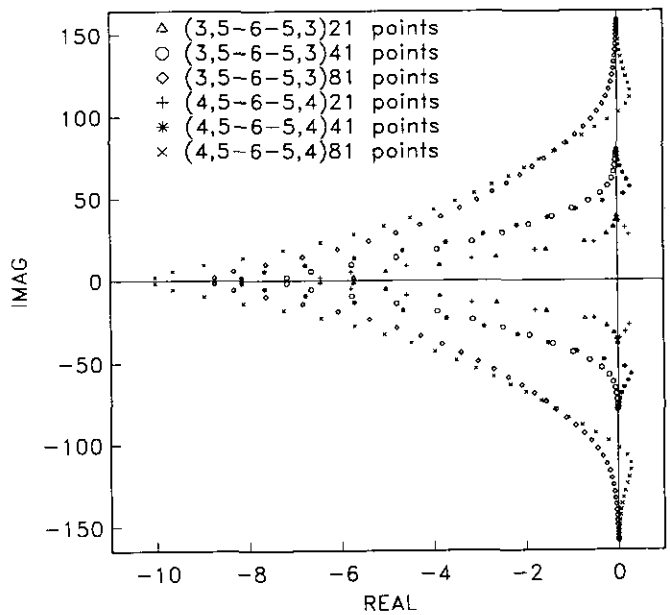

FIG. 8. Numerically determined eigenvalue spectrum from sixth-order Padé inner scheme, closed with either third- or fourth-order boundary schemes.

TABLE IV

Numerical versus Theoretical Growth Rate
for (4, 5–6–5, 4) Scheme

Grid	$\gamma_{\text{Numerical}}$	$\gamma_{\mathscr{R}(S_{\max})}$
21	0.1245	0.1228
41	0.1402	0.1381
81	0.1351	0.1354

either the fourth-order time or the fifth-order space truncation terms.) The amplification is accurately predicted by the eigenvalue determination. Table IV compares the numerical amplification rate $\gamma_{\text{Numerical}}$ with that obtained theoretically with $\mathscr{R}(S_{\max})$. The agreement is excellent.

The preceding examples of sixth-order schemes show the strength of G–K–S analysis for accurate prediction of the stability of complex, higher order schemes. These examples also show the intimate relationship between the eigenvalues of the spatial operator and the stability of the resulting scheme.

We now present formally the sixth-order accurate schemes that are closed at the boundaries by at least fifth-order stencils. Our first attempt is with optimal fifth-order closure at the boundaries, which results in the scheme (5, 5–6–5, 5). Figure 10 shows the error of the simulation of the scalar wave equation defined by Eqs. (23)–(25). The behavior of this scheme is fundamentally different from the (4, 5–6–5, 4) scheme in several ways. On all grids, the error always increases monotonically in time. For CFLs near the theoretical maximum value, the error increases at a lower rate, but it is not suppressed as with the lower order schemes. In addition, the exponential growth rate of the error increases as the grid density increases. On the grids shown, the error in the solution could not be systematically reduced by refining the grid and repeating the calculation to a specified time level T. In spite of these differences, the eigenvalue determination still accurately predicts the growth of the solution. Table V shows a comparison of the numerical and theoretical amplification rates. The theoretical values are determined from the $\mathscr{R}(S_{\max})$ for each grid.

Again, the agreement is excellent. The solution grows at a rate that, for long times, is dominated by the eigenvalue with the maximum real part. The eigenvalue determination accurately predicts the behavior of the numerical solution, even for this case, which appears not to be Lax stable.

Figure 11 shows a plot of the eigenvalue spectrum for the (5, 5–6–5, 5) scheme on grids of 21, 41, and 81 points. The $\mathscr{R}(S_{\max})$ obviously increases for these grids and appears to increase without bound (as opposed to an asymptotic limit), which violates a necessary condition for Lax stability. As in the (3^1, 5–6–5, 3^1) example, a precise conclusion cannot be drawn from grid-refined eigenvalue determination, although the trends have been the same in the cases presented thus far. G–K–S stability theory must ultimately be relied upon to determine if the scheme is stable.

We begin by determining the stability of the outflow boundary for the (5, 5–6–5, 5) scheme. The quarter-plane problem appropriate for this analysis is that described in Eq. (81). No boundary conditions are necessary, but NBSs

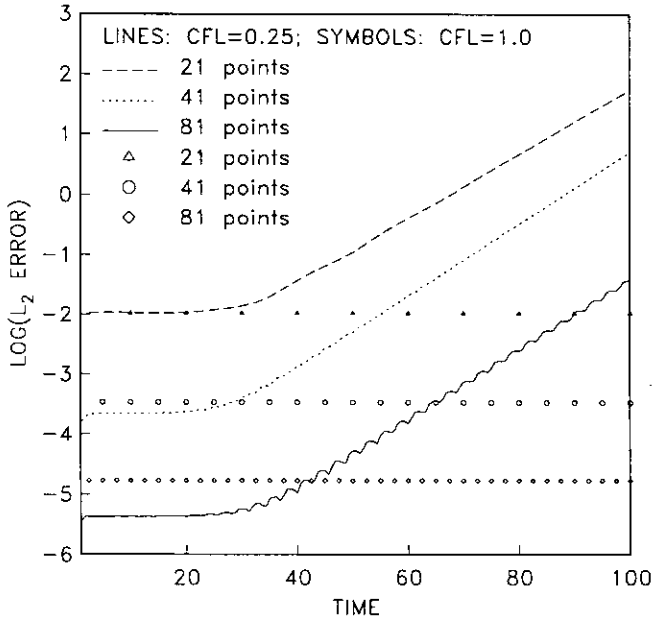

FIG. 9. The L_2 error as a function of time from uniformly sixth-order Padé scheme with fourth-order boundary closure (4, 5–6–5, 4) for various CFLs and grid densities.

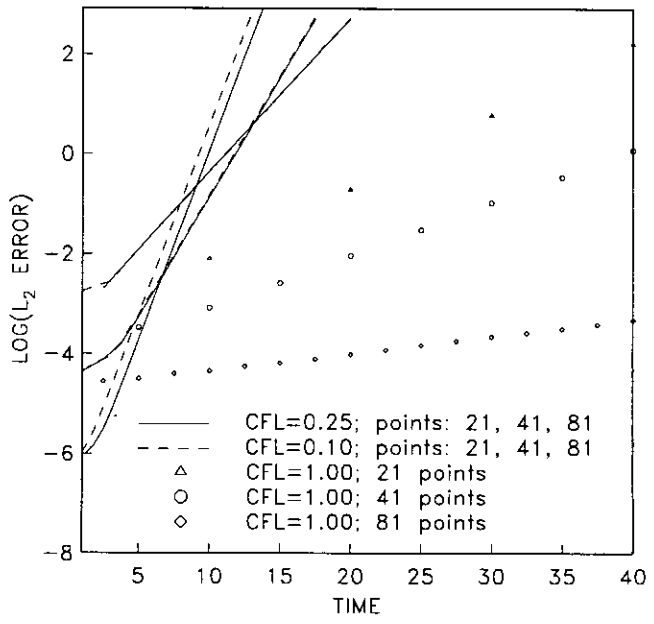

FIG. 10. The L_2 error as a function of time from uniformly sixth-order Padé scheme with fifth-order boundary closure (5, 5–6–5, 5) for various CFLs and grid densities.

TABLE V

Numerical versus Theoretical Growth Rate
for (5, 5–6–5, 5) Scheme

Grid	$\gamma_{\text{Numerical}}$	$\gamma_{\mathcal{R}(S_{\max})}$
21	0.7121	0.7138
41	1.104	1.010
81	1.749	1.742

are used at grid points $j=0, 1$. The closure at grid point $j=0$ is accomplished with

$$\frac{\partial U_0}{\partial x}+4\frac{\partial U_1}{\partial x}=\frac{1}{12\,\Delta x}(-37U_0+8U_1+36U_2-8U_3+U_4) \tag{109}$$

while that of grid point $j=1$ is accomplished with Eq. (93). Solutions of the form $U_j(t)=e^{St}\phi_0\kappa^j$ will satisfy the numerical scheme, which gives the sixth-order inner scheme the resolvent condition shown in Eq. (95). The fourth-order polynomial in κ will have two roots that are $|\kappa|\leqslant 1$, and the general solution will have the form $U_j(t)=e^{St}(C_1\kappa_1^j+C_2\kappa_2^j)$. This expression is substituted into the two boundary conditions to yield boundary expressions for the constants C_1 and C_2 of the form

$$\begin{aligned} C_1F_0(\kappa_1)+C_2F_0(\kappa_2)&=0\\ C_1F_1(\kappa_1)+C_2F_1(\kappa_2)&=0, \end{aligned} \tag{110}$$

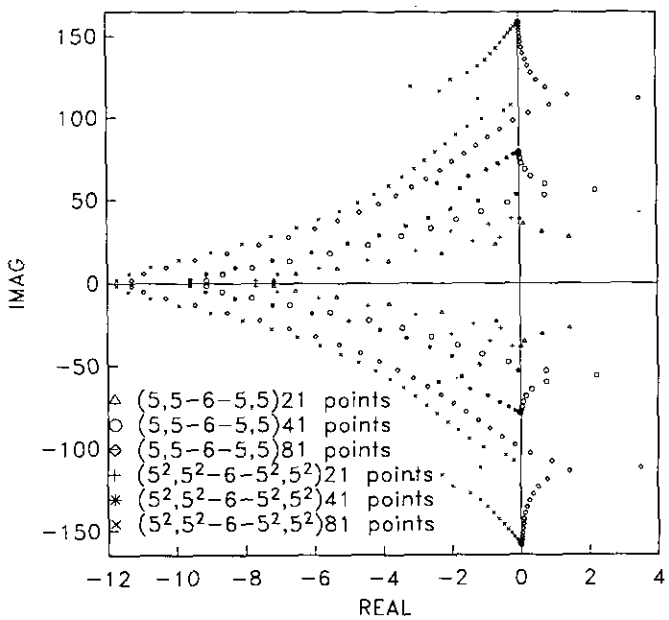

FIG. 11. Numerically determined eigenvalue spectrum from sixth-order Padé inner scheme, closed with conventional fifth- or newly developed fifth-order boundary schemes.

where

$$\begin{aligned} F_0(\kappa)&=(1+4\kappa_1)\,\hat{S}-(-37+8\kappa+36\kappa^2-8\kappa^3+\kappa^4)/12\\ F_1(\kappa)&=(1+6\kappa+3\kappa^2)\,\hat{S}-(-10-9\kappa+18\kappa^2+\kappa^3)/3. \end{aligned} \tag{111}$$

Equation (110) can only have a nontrivial solution if the determinant condition $F_0(\kappa_1)F_1(\kappa_2)-F_1(\kappa_2)F_0(\kappa_1)=0$ is satisfied. The resolvent condition equation (95) is solved for $\hat{S}$ and substituted into the determinant condition to produce

$$\frac{(\kappa_1-1)^4(\kappa_2-1)^4(\kappa_2-\kappa_1)(4\kappa_2\kappa_1+\kappa_2+\kappa_1-6)}{144\kappa_1\kappa_2(\kappa_1^2+3\kappa_1+1)(\kappa_2^2+3\kappa_2+1)}=0. \tag{112}$$

Equation (112) is solved to yield $\kappa_1=1$, $\kappa_2=1$, $\kappa_1=\kappa_2$, or the expression

$$\kappa_1=-\frac{\kappa_2-6}{4\kappa_2+1}. \tag{113}$$

The first two roots are the same roots that have previously been shown to be stable. The condition that both roots must be $|\kappa|\leqslant 1$ precludes the last root. The third root can be shown to be stable by testing the derivative condition of the polynomial as follows. Multiplication and division of Eq. (110) by the nonzero rows and columns does not change the roots of the determinant conditions. The resulting expression is

$$\begin{vmatrix} F_0(\kappa_1) & \dfrac{F_0(\kappa_2)-F_0(\kappa_1)}{\kappa_2-\kappa_1}\\ F_1(\kappa_1) & \dfrac{F_1(\kappa_2)-F_1(\kappa_2)}{\kappa_2-\kappa_1} \end{vmatrix}=0.$$

The limit as $\kappa_1\to\kappa_2$ is taken to yield the expression for the determinant condition $F_0(\kappa)(dF_1(\kappa)/d\kappa)-F_1(\kappa)(dF_0(\kappa)/d\kappa)=0$. The resulting expression for κ is

$$\frac{(\kappa-1)^{12}}{144\kappa^2(\kappa^2+3\kappa+1)^2}=0. \tag{114}$$

Thus, the outflow boundary is stable for the (5, 5–6–5, 5) scheme.

The model equation for the inflow quarter-plane problem is the same as that described in Eqs. (85) and (86). Solutions of the form $U_j(t)=e^{St}\phi_0\kappa^j$ will satisfy the numerical scheme, which gives the sixth-order inner scheme the same resolvent condition as in Eq. (101). Again, the general solution will have the form $U_j(t)=e^{St}(C_1\kappa_1^j+C_2\kappa_2^j)$. This expression is substituted into the two boundary conditions

and $U_0 = 0$, which produces two equations for the constants C_1 and C_2 of the form

$$\begin{aligned} C_1 F_1(\kappa_1) + C_2 F_1(\kappa_2) &= 0 \\ C_1 F_2(\kappa_1) + C_2 F_2(\kappa_2) &= 0, \end{aligned} \tag{115}$$

where

$$\begin{aligned} F_1(\kappa) &= (2\kappa + 3\kappa^2)\,\hat{S} - (+44\kappa - 36\kappa^2 - 12\kappa^3 + \kappa^4)/12 \\ F_2(\kappa) &= 1. \end{aligned} \tag{116}$$

The determinant condition, for which a nontrivial solution exists is simplified to $F_1(\kappa_1) - F_1(\kappa_2) = 0$ and, with Eq. (100), provides two equations for the two unknowns κ_1 and κ_2. With the change of variables $\kappa_1 + \kappa_2 = 2y$ and $\kappa_1 \kappa_2 = x$, Eq. (116) becomes

$$\begin{aligned} &-64y^5 + (192 - 96x)\,y^4 + (-16x^2 + 352x - 240)\,y^3 \\ &\quad + (120x^2 - 504x + 160)\,y^2 + (8x^3 - 216x^2 + 360x - 56)\,y \\ &\quad - 18x^3 + 142x^2 - 142x + 18 = 0. \end{aligned} \tag{117}$$

The functional relationship $y = y(x)$ provided by Eq. (108) is substituted into Eq. (117) and simplified to yield

$$\begin{aligned} &(x-1)(x+1)^5\,(x^{12} + 261x^{11} + 24298x^{10} \\ &\quad + 864903x^9 + 5558711x^8 + 16502410x^7 \\ &\quad + 27479264x^6 + 28538822x^5 + 5255107x^4 \\ &\quad + 429169x^3 + 18614x^2 + 435x + 5) = 0. \end{aligned} \tag{118}$$

Two roots to this polynomial give rise to eigenvalues $\hat{S}$ that are in the RH-P. They are $x = (-0.0196916 \pm 0.0239802i)$, which yields $\kappa_1 = (0.157055, \mp 0.943601i)$, and $\kappa_2 = (-0.0281082, \mp 0.0161902i)$, for $\hat{S} = (0.0428389, \pm 1.39944i)$. The numerical solutions satisfy the governing equations to approximately machine precision (1.0e − 13). Thus, the inflow for the (5, 5–6–5, 5) scheme is G–K–S unstable. This result verifies the trends indicated earlier by the eigenvalue grid refinement analysis and the simulation of the scalar wave equation, both of which indicated that the sixth-order scheme was Lax unstable.

The unstable scheme (5, 5–6–5, 5) previously discussed was implemented with optimal fifth-order boundary formulas. If the constraint of optimal-order schemes at the boundaries is relaxed, then the possibility of a fifth-order closure that is G–K–S stable still exists. Taylor series truncation analysis was used to develop parametric relations for the closure formulas at the two NBSs. These parametric relations were constrained to be fifth order and explicit in nature. To facilitate a wide range of closures, each point was given two degrees of freedom. Thus, the symbolic formula for the new scheme is (5^2, 5^2–6–5^2, 5^2). The scheme defined at grid point $j = 0$ and 1 can be writen as

$$\begin{aligned} \frac{\partial U_0}{\partial x} = \frac{1}{\Delta x} &(C_0 U_0 + C_1 U_1 + C_2 U_2 + C_3 U_3 + C_4 U_4 \\ &+ C_5 U_5 + C_6 U_6 + C_7 U_7) \end{aligned} \tag{119}$$

$$\begin{aligned} \frac{\partial U_1}{\partial x} = \frac{1}{\Delta x} &(D_0 U_0 + D_1 U_1 + D_2 U_2 + D_3 U_3 + D_4 U_4 \\ &+ D_5 U_5 + D_6 U_6 + D_7 U_7), \end{aligned} \tag{120}$$

where

$$\begin{aligned} C_0 &= -(\alpha_0 - 28\beta_0 + 13068)/5040 \\ C_1 &= +(\alpha_0 - 27\beta_0 + 5040)/720 \\ C_2 &= -(\alpha_0 - 26\beta_0 + 2520)/240 \\ C_3 &= +(\alpha_0 - 25\beta_0 + 1680)/144 \\ C_4 &= -(\alpha_0 - 24\beta_0 + 1260)/144 \\ C_5 &= +(\alpha_0 - 23\beta_0 + 1008)/240 \\ C_6 &= -(\alpha_0 - 22\beta_0 + 840)/720 \\ C_7 &= +(\alpha_0 - 21\beta_0 + 720)/5040 \\ D_0 &= -(\alpha_1 - 21\beta_1 + 720)/5040 \\ D_1 &= +(\alpha_1 - 20\beta_1 - 1044)/720 \\ D_2 &= -(\alpha_1 - 19\beta_1 - 720)/240 \\ D_3 &= +(\alpha_1 - 18\beta_1 - 360)/144 \\ D_4 &= -(\alpha_1 - 17\beta_1 - 240)/144 \\ D_5 &= +(\alpha_1 - 16\beta_1 - 180)/240 \\ D_6 &= -(\alpha_1 - 15\beta_1 - 144)/720 \\ D_7 &= +(\alpha_1 - 14\beta_1 - 120)/5040 \end{aligned}$$

with similar expressions defined for the closure at the other end of the domain. By systematically searching the four-parameter space spanned by the parameters α_0, β_0, α_1, and β_1 with an eigenvalue code, an arbitrary eigenvalue spectrum can be approximated. A particular set of coefficients for which the eigenvalue spectrum is bounded to the LH-P is $\alpha_0 = 1809.257$, $\beta_0 = -65.1944$, $\alpha_1 = -262.16$, and $\beta_1 = -26.6742$. The values are not unique and no attempt has been made to find optimal values for these coefficients. The eigenvalue spectrum for this case is shown in Fig. 11. Note that the shape of the spectrum is similar to that of the (5, 5–6–5, 5) scheme, but that the $\mathcal{R}(S_{\max}) \leqslant 0$ instead of increasing without bound. The scheme satisfies the necessary condition for Lax stability and is asymptotically stable by our definitions.

The stability analysis for the two quarter-plane problems that establish the G–K–S stability of the new (5^2, 5^2–6–5^2, 5^2) scheme is extremely formidable; MACSYMA is pushed to the limits of its capabilities on present machines. In addition, 128-bit arithmetic is required to ensure precision in the determination of the roots of the resulting polynomials in x. The scheme is G–K–S stable for the parameters given above for the inflow and outflow problems. Thus, a formally sixth-order scheme has been developed that is G–K–S (Lax) stable and asymptotically stable for the scalar case.

Table VI shows a grid refinement study performed with the new sixth-order scheme to verify its accuracy. The model problem is the scalar wave equation defined by Eqs. (23)–(25). The time-advancement scheme is the fourth-order R–K algorithm with a CFL of 0.1. Temporal refinement studies were performed to ensure that the leading error terms on all grids were from the spatial discretization operator. The grid, its error, and the slope between each successive refinement are listed in the table. The asymptotic stability of the spatial operator ensures that the solution does not grow exponentially for long times.

In Table VI, the data point for 21 grid points is erroneous because the grid is too coarse for the scheme to exhibit its higher order properties. In this example, the scheme becomes at least fifth-order accurate at approximately 10 grid points/2π rad. In the limit $N \to \infty$, where N is the number of grid points, the scheme shows a slope of -6, which is the formal accuracy of the inner scheme. For small values of N, the four points that are treated with fifth-order accuracy degrade the formal accuracy by one degree.

An asymptotically stable, sixth-order spatially accurate scheme has been developed for use in a method-of-lines discretization of a hyperbolic partial differential equation. The eigenvalues of the new scheme are for the scalar case, which is bounded to the LH-P for all N. The necessary condition for Lax stability is therefore satisfied. In addition, the scheme has been shown to be G–K–S stable for the combined inflow and outflow quarter-plane analysis and is therefore formally Lax stable for the scalar case.

TABLE VI

Grid Refinement Study of the (5^2, 5^2–6–5^2, 5^2) Scheme

Grid	$\log(L_2)$ rate	Slope
21	−2.363	NA
31	−3.582	−6.9
41	−4.225	−5.1
51	−4.724	−5.1
61	−5.150	−5.4
81	−5.849	−5.6
101	−6.406	−5.7
121	−6.867	−5.8

For the hyperbolic system of equations, the use of any of the Lax stable schemes presented in this work guarantees the Lax stability of the resulting spatial discretization when the boundaries are imposed in characteristic form. The concept of asymptotic stability does not carry over from the scalar case to the system. For the system, when all of the physical eigenvalues have the same sign, the asymptotic stability is retained. When the eigenvalue signs are mixed, although asymptotically stable for the scalar case, exponential growth of the solution may occur for boundaries that are imposed in characteristic form. Research continues to determine a stronger necessary condition for asymptotic stability that will allow the use of scalar analysis to determine spatial schemes that are asymptotically stable for the system.

CONCLUSIONS

The stability characteristics of various compact fourth- and sixth-order spatial operators were assessed with the theory of Gustafsson, Kreiss, and Sundström (G–K–S) for the semidiscrete initial boundary value problem (IBVP). The class of central-difference interior schemes with asymmetrically closed boundaries was analyzed. Because of formal accuracy considerations, those schemes with boundary closures of at least $(N-1)$th spatial order for an (N)th-order inner scheme were the focus of the work. Conventional third- or fourth-order boundary conditions, when coupled with the fourth-order compact inner scheme, resulted in a G–K–S stable scheme. For the sixth-order compact inner scheme, the conventional boundary closures of fifth and higher order were found to be G–K–S unstable. Fourth-order and lower order closure formulas were found to be G–K–S stable. These results were then generalized to the fully discrete case with a recently developed theory of Kreiss, which states that under weak constraints, the stability of the semidiscrete operator implies stability of the fully discrete operator if a locally stable temporal method is used.

The conventional definition of stability was then sharpened to include only those spatial discretizations that are asymptotically stable (bounded left half-plane (LH-P) eigenvalues). Many of the higher order schemes which are G–K–S stable were found not to be asymptotically stable. Fourth-order boundary conditions were found to be asymptotically unstable for the schemes tested, specifically: (4–4–4) and (4, 5–6–5, 4). A series of compact fourth- and sixth-order schemes that were both asymptotically and G–K–S stable were then developed. The constraint of optimal accuracy from a specific number of constraints was abandoned, which enabled several-parameter boundary closures to be developed. A three-parameter, uniformly

fourth-order scheme (4^3–4–4^3) and a four-parameter sixth-order scheme with fifth-order boundaries (5^2, 5^2–6–5^2, 5^2) were developed which were asymptotically stable. No attempt was made to optimize the parameters.

All the schemes that were G–K–S stable were subjected to extensive comparisons between the G–K–S stability predictions, semidiscrete eigenvalue determination, and numerical simulations. In all cases, consistent and complementary results were achieved with all the methods. In addition, the eigenvalue determination accurately predicted the exponential divergence of the solution for the cases that were not asymptotically stable. Table VII presents a summary of the results.

TABLE VII

Stability of High Order Discretizations for $U_t = aU$ with Various Boundary Conditions

Order	Scheme	Type	G–K–S	$\mathrm{Re}(S) \leqslant 0$
2nd	1–2–1	Explicit	Yes	Yes
2nd	2–2–2	Explicit	Yes	Yes
2nd	1, 1–4–1, 1	Explicit	Yes	Yes
3rd	2, 2–4–2, 2	Explicit	Yes	Yes
4th	3, 3–4–3, 3	Explicit	Yes	Yes
4th	4, 4–4–4, 4	Explicit	Yes	No
2nd	1–4–1	Compact	Yes	Yes
3rd	2–4–2	Compact	Yes	Yes
4th	3–4–3	Compact	Yes	Yes
4th	4–4–4	Compact	Yes	No
4th	4^3–4–4^3	Compact	Yes	Yes
4th	3, 4–6–4, 3	Compact	Yes	Yes
5th	4, 4–6–4, 4	Compact	Yes	No
6th	5, 5–6–5, 5	Compact	No	No
6th	5^2, 5^2–6–5^2, 5^2	Compact	Yes	Yes

REFERENCES

1. Z. Kopal, *Numerical Analysis*, 2nd ed. (Wiley, New York, 1961).
2. R. Vichnevetsky and J. B. Bowles, *Fourier Analysis of Numerical Approximations of Hyperbolic Equations* (SIAM, Philadelphia, 1982).
3. B. Gustafsson, *Math. Comput.* **29**, No. 130, 396 (1975).
4. S. Osher, *Trans. Amer. Math. Soc.* **137**, 177 (1969).
5. H.-O. Kreiss, *Commun. Pure Appl. Math.* **23**, 277 (1970).
6. B. Gustafsson, H.-O. Kreiss, and A. Sundström, *Math. Comput.* **26**, 649 (1972).
7. L. N. Trefethen, *J. Comput. Phys.* **49**, 199 (1983).
8. J. C. Strikwerda, *J. Comput. Phys.* **34**, 94 (1980).
9. M. Goldberg and E. Tadmor, *Math. Comput.* **48**, No. 178, 503 (1987).
10. H.-O. Kreiss and L. Wu, Technical report, Dept. of Mathematics, UCLA, 1989; *Commun Pure Appl. Math.*, to appear.
11. D. Gottlieb, M. Gunzburger, and E. Turkel, *SIAM J. Numer. Anal.* **19**, No. 4 (1982).
12. J. Gary, *J. Comput. Phys.* **26**, 339 (1978).
13. C. W. Gear, *Numerical Initial Value Problems in Ordinary Differential Equations* (Prentice–Hall, Englewood Cliffs, NJ, 1971).
14. M. W. Hirsch and S. Smale, *Differential Equations, Dynamical Systems, and Linear Algebra* (Academic Press, New York/London, 1974).
15. R. C. Reddy and L. N. Trefethen, "Lax-Stability of Fully Discrete Spectral Methods via Stability Regions and Pseudo-Eigenvalues," in *Proceedings, ICOSAHOM Conference on Spectral and High Order Methods for Partial Differential Equations, 1989* (North-Holland, Amsterdam, 1989).
16. S. K. Lele, *J. Comput. Phys.* **103**, 16 (1992).